Geothermics 134 (2026) 103525

Contents lists available at ScienceDirect

Geothermics

journal homepage: www.elsevier.com/locate/geothermics

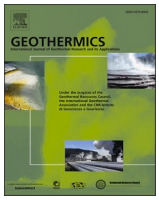

Thermal response of heterolithic deposits in flooded coal mines: implication for heat storage potential

Mylene Receveur [a,*], Andres Gonzalez Quiros [a], Alison Monaghan [a], Vanessa Starcher [a], Kyle Walker-Verkuil [a], David Boon [a], Jeroen van-Hunen [b]

[a] British Geological Survey, The Lyell Centre, Research Avenue South, Edinburgh, United Kingdom
[b] Durham University, Stockton Road, Durham DH1 3LE, United Kingdom

ARTICLE INFO

Keywords:
Mine water geothermal
Heat storage
Distributed temperature sensing
Numerical modelling
UK Geoenergy Observatory Glasgow

ABSTRACT

Heat transfer rates are critical to underground heat storage recovery potential and sustainability of thermal abstraction for heating and cooling buildings. A 17-day heat injection – abstraction experiment into a flooded, disused mine working was conducted at the UK Geoenergy Observatory in Glasgow. Analysis of the thermal response of different lithologies intersected by an injection borehole during and after a heat injection experiment is used to quantify the heat exchange between rock mass and circulating mine water. The monitoring data from Distributed Temperature Sensing (DTS) has been analysed and numerical models using COMSOL Multiphysics were developed to characterise the rates and controls on thermal processes during heat injection and recovery. The results suggest the key control of the borehole construction on the temperature change in the first 10 hour of heat injection. In the long term, the thermal response mainly depends on the thermal conductivity of the lithologies. The radial heat transfer reaches a steady charging rate of 23 W/m^2 and 16 W/m^2 in the sandstone and clay intervals, respectively, and a maximum of 14 W/m^2 and 10 W/m^2 at the start of recovery. This is accompanied by upward heat diffusion/convection from the mine working. This study demonstrates the ability of DTS to identify lithological heterogeneities at a high resolution, and the importance of considering the overburden structure and lithology for thermal storage applications.

1. Introduction

The low-temperature geothermal resources contained in flooded coal mines have the potential to contribute to the decarbonisation of residential and industrial heating and cooling in the former mining regions globally (Walls et al., 2021). Mine water reservoirs can store a large volume of water, which can be extracted at relatively high rates, provided the mining voids are interconnected over large areas and have the appropriate hydraulic properties (Bailey et al., 2013). Mine water temperature in the UK typically ranges between 12°C and 20°C (Farr et al., 2021). Using a heat pump system, the low-grade heat can be raised to useful temperatures for space heating and hot water applications (Gillespie et al., 2013, Watzlaf and Ackman, 2006). In the UK, about 23,000 flooded coal mines provide a vast amount of subsurface water resource capable of storing substantial quantities of heat. About 25 % of the population in the UK lives in former mining areas (Gluyas et al., 2020), with 9 out of the 10 largest urban centres being underlain by mine workings, and could directly benefit from this local and low carbon energy source.

In addition to using mine water as a heat source, mines have been increasingly considered for their thermal energy storage potential (Menéndez et al., 2019). Mine Thermal Energy Storage (MTES) is a technology that uses flooded mine for seasonal heat storage through the injection and abstraction of water, used as the heat carrier (Li et al., 2020, Ngoyo Mandemvo et al., 2023, Ferket et al., 2011). Depending on the volume of interconnected voids, the circulating mine water has the potential to access a large extent of the mine, storing and extracting heat via heat exchange with the surrounding rock mass (Ordóñez et al., 2012). Closed-loop systems (e.g. Borehole Thermal Energy Storage, BTES) are an alternative option the water circulates in a U-tube heat exchanger inserted in a borehole or shaft. Heat is stored into / extracted from the subsurface via diffusive heat transfers between the borehole walls and the surrounding rock mass (Brown et al., 2024).

For both geothermal and storage utilisation, understanding the

* Corresponding author.
E-mail address: mreceveur@bgs.ac.uk (M. Receveur).

https://doi.org/10.1016/j.geothermics.2025.103525
Received 31 July 2025; Received in revised form 16 September 2025; Accepted 4 November 2025
Available online 14 November 2025
0375-6505/© 2025 British Geological Survey, a component body of UKRI. 'BRITISH GEOLOGICAL (C) UKRI. All Rights Reserved'. Published by Elsevier Ltd. This is an open access article under the CC BY license (http://creativecommons.org/licenses/by/4.0/).

reservoir structure (i.e., the mine workings and overlying rock mass), the hydrogeology and the thermal properties of the subsurface is essential but generally challenging in mining environments (Monaghan et al., 2026). The underground mining voids left from the mining activities tend to form a complex interconnected network of mine workings, galleries, shafts and roadways that might remain open, partially open or closed following the closure of the mine (Younger et al., 2002, Andrews et al., 2020). Subsequent subsidence, fracturing and collapse of the roof may also impact the distribution of the mining voids and the hydraulic and thermal properties in both the mine workings and overlying rock mass, which may disturb the flow of water and the transport of heat (Ferket et al., 2011, Adams and Younger, 2001). One of the key limitations to the characterisation of the hydraulic and thermal behaviour of such system lies in the sparsity of direct observations of the flow and heat transport processes (i.e. borehole or shaft access for measurements), both over the spatial extent of the interconnected parts of a mine and over time, and the difficulty of obtaining in-situ measurement of the material properties (Farr et al., 2021). The lack of understanding on the heat sources and heat transfer processes limits accurate estimation of the long-term efficiency and sustainability that underpin business cases for deployment of mine water energy systems.

Previous research on MTES has suffered from the lack of field and operational data, with numerical modelling studies generally focusing on conceptual representations of mine workings (Perez Silva et al., 2022, Todd et al., 2024). Currently, various projects are evaluating the potential of thermal energy storage in mines, including high-temperature thermal storage, and providing data from highly instrumented at-scale infrastructures from demonstrator and research sites (Gonzalez Quiros et al., 2025b, Passamonti et al., 2024, Passamonti et al., 2025, Atkinson et al., 2024, Fraser-Harris et al., 2022, Monaghan et al., 2026). These offer new opportunities to gain a better understanding of the thermal processes involved in mine water energy systems.

This work aims at better characterising and understanding the storage and heat recovery potential of key lithologies in the Carboniferous Coal Measures, using Distributed Temperature Sensing (DTS) data collected at the UK Geoenergy Observatory in Glasgow (UKGEOS) during a 17-day heat injection experiment and subsequent one-week recovery period. DTS is a method that uses fibre optic (FO) cables to produce a continuous profile of in-situ temperature, which can be used to infer the hydrogeological and geothermal properties of the subsurface, such as the flow pattern from naturally occurring thermal anomalies. DTS has received growing attention in recent years as the technology improved into providing finer temporal, spatial, and temperature resolution. Examples of applications include the analysis of groundwater/surface water interactions (Lowry et al., 2007, Slater et al., 2010, Blume et al., 2013, Leaf, 2020), soil moisture content (Steele-Dunne et al., 2010, Sayde et al., 2010), lake thermal stratification (Suárez et al., 2011, Arnon et al., 2016) and estimation of subsurface hydraulic properties (Read et al., 2014). In an active underground mine environment, DTS has been used to measure air temperature and determine the rate of heat generation in order to ensure the safety of underground miners (Aminossadati et al., 2010) and detect the onset of coal spontaneous combustion in goaf (Zhang et al., 2023, Duarte et al., 2022). In geothermal research, DTS has been used to record temperature gradients (McDaniel et al., 2018, Cottingham et al., 2013), analyse in situ subsurface thermophysical properties (Henninges et al., 2005, Freifeld et al., 2008, Simon et al., 2021) and ground heat exchanger performance (Fujii et al., 2009, Beier et al., 2012, Acuña and Palm, 2013).

In this work, we use the high spatial and temporal resolution of temperature measurements provided by the DTS cables installed on the outside of the injection borehole casing (Fig. 1) to constrain the

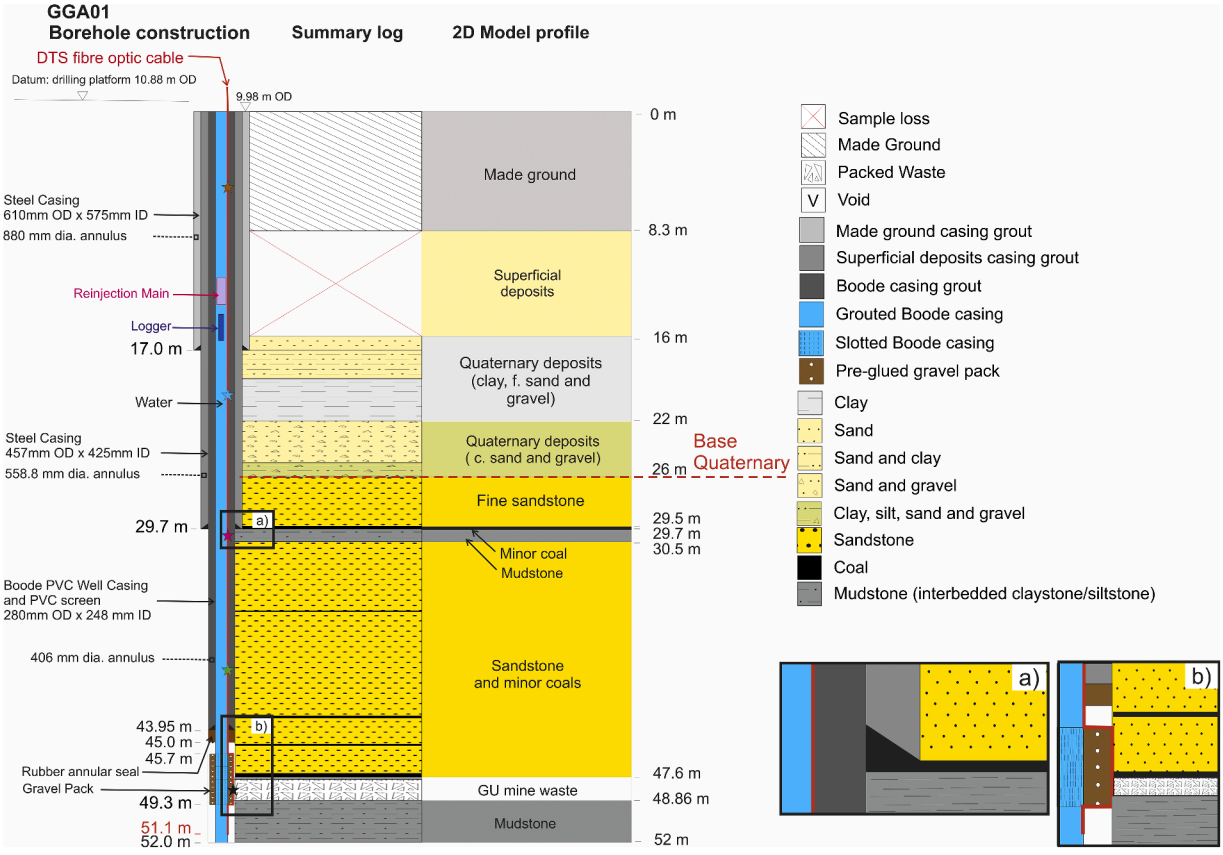

Fig. 1. Conceptual representation of the lithological succession intersected by borehole GGA01, showing the borehole construction, the borehole materials and the location of the FO-DTS cable. Zooms a) at c. 30 m depth in the mudstone interval and b) at the GU depth interval.

properties of the rock mass overlying the mine workings and analyse the effect of reservoir heterogeneities and borehole construction on the measured thermal response. The interpretation of the experimental data collected during the heat injection experiment is supported by numerical analyses. These are used to investigate the sensitivity of the temperature observed along the injection borehole to a range of borehole material and subsurface properties, characterise the main heat transfer processes and the thermal recovery rate. This experiment takes advantage of the capabilities of the Observatory with an unprecedented level of monitoring that allowed the detection of thermal breakthrough in the abstraction borehole (Gonzalez Quiros et al., 2025a). The data recorded during and after the heat injection experiment provides valuable information on the heat recovery potential and unique opportunities to characterise the long-term sustainability of mine water geothermal and seasonal thermal energy storage. This is, to the best of our knowledge, the first time DTS attached to the exterior of the borehole is used to monitor a heat injection experiment for mine water geothermal research and in-situ estimation of thermal properties.

2. Methodology

2.1. UK Geoenergy Observatory infrastructure

2.1.1. Site description

The UK Geoenergy Observatory (UKGEOS) is an at-scale research and monitoring site built with the aim to de-risk the development of mine water geothermal resources in the UK and worldwide (Monaghan et al., 2022a). It is located on the western side of the Central Coalfield in the Midland Valley of Scotland and accesses the flooded mine workings of Farme colliery at the Cuningar Loop in Glasgow (see location map in Monaghan et al. (2022b)).The geological succession typically consists of superficial Quaternary deposits down to about 26 m depth, overlying about 300 m of Scottish Coal Measures Group bedrock, Westphalian in age, in which a total of seven coal seams have been worked between 1805 and 1928 (Findlay et al., 2020). Below this succession are the Carboniferous strata of the Clackmannan and Strathclyde groups (Browne and McMillan, 1989).

The Observatory has been constructed at the scale of a small-medium mine energy scheme with the aim of improving scientific understanding of mine water geothermal systems, de-risking exploitation, and evaluating the long-term sustainability of mine-water geothermal resource (Monaghan et al., 2022a, 2022b). The similarities between the geological, mining and operational characteristics of the infrastructure with other commercial projects in the UK and worldwide provides opportunities to test response to induced changes of flow and heat under various scenarios, which would not be possible within commercial schemes (Monaghan et al., 2022a). Among the eleven boreholes drilled at the Cuningar Loop, five of them are mine water boreholes, accessing either the Glasgow Upper (GU) or the Glasgow Main (GMA) mine workings, both characterised by different hydrogeological conditions (Gonzalez Quiros et al., 2024). In the experiment described in this study (see Section 2.2), the boreholes GGA01 and GGA07 located 135 m apart and both accessing the GU mine workings at a depth of c. 50 m, were used as injection and abstraction wells, respectively. In addition to the mine workings boreholes, five environmental monitoring boreholes drilled into superficial deposits or bedrock above the GU are used to characterise the baseline conditions and monitor the impact of the geothermal operations.

2.1.2. GGA01 borehole design

Considerations of the borehole design are essential to understand the impact of the construction characteristics on the thermal response recorded by DTS. Here, we provide an overview of the 52 m deep borehole GGA01 used in the heat injection experiment (Fig. 1).

The borehole consists of three casings installed through the made ground (steel made ground casing), superficial deposits (steel rockhead casing) and bedrock (PVC Boode Well casing) down to 17 m, 29.7 m and 45.7 m depth, respectively (Monaghan et al. 2021). The annulus of the different casing sections was grouted before the next section was drilled. The borehole is only screened across the GU mine working, intersected between 47.60 m and 48.86 m, with the slotted screen and gravel pack extending from 45.7 to 49.3 m. The borehole is fully sealed above the screen, so that all hydrogeological observations only relate to this interval. The large internal diameters of Boode Well casing and slotted screen section (248 mm Internal Diameter (ID)) were chosen to accommodate a large submersible pump capable of delivering a flow rate of up to 12 l/s.

GGA01 is equipped with a fibre-optic distributed temperature sensing (FO-DTS) cable, installed on to the outside of the 11″ (280 mm OD) Boode Well casing and across the screened section, down to a depth of 51.1 m below ground level (Fig. 1). The cable includes two Stranded Copper Wires and four Multi Mode (MM) fibres that are comprised of 2 MM loops. The cable end is located at 0.9 m above the casing shoe. It was placed onto the casing and fastened into position before lowering the equipment down the borehole. The borehole annulus between the Boode Well casing and rock wall (i.e. 406 mm diameter hole) was grouted above the screened section and around the FO-DTS cables, representing a grout thickness of 63 mm in the lower part of the borehole (Monaghan et al., 2022b, Maciver, 2019).

2.1.3. Lithological description

The lithological succession in GGA01 has been described in Monaghan et al. (2020) and is displayed in the simplified diagram (Fig. 1). The top part of the stratigraphy consists of about 8.3 m of made ground, defined as artificial deposits composed of sand, silt, gravel and boulders in which brickwork, roots, wood planks, glass fragments and plastic have been found. These are underlain by Quaternary deposits, typically formed of unconsolidated sediments including sand, pebble, gravel and the Paisley Clay Member, consisting of a clay-dominated interval between 19 m and 22 m (Monaghan et al., 2020, Monaghan et al., 2022b). The Paisley Clay Member was identified as the key unit separating the mine water aquifer and the superficial aquifer (Gonzalez Quiros et al., 2024). No sample was collected from the made ground and superficial deposits down to the first casing point at 16 m depth and therefore no information is available to constrain the model developed in this analysis from GGA01. At 26 m depth, the Quaternary deposits lie unconformably on the Carboniferous Scottish Middle Coal Measures Formation, which has been extensively mined for coal. The upper part of the Carboniferous bedrock succession, above the GU mine working, is dominated by fine- to medium-grained sandstone with alternating siltstone, mudstone and minor unmined coal layers. A mudstone layer dominates the succession below the GU mine working and down to the bottom of the GGA01 borehole. Between 47.60 m and 48.86 m depth, the GU mine working was described by Monaghan et al. (2022a) as being dominated by packed backfilled mine waste. The type of mine workings however varies across the Farme Colliery. Intact pillars, total extraction areas, open voids, roadways, waste and stowage within the mining units as well as fractured rocks have been intersected by other mine workings boreholes, suggesting a heterogeneous and complex hydrogeological system.

This study looks at the thermal response of entire lithological succession and more particularly at the depth of the Paisley Clay Member at c. 20 m, a Carboniferous mudstone interval with a minor coal layer at c. 30 m and a sandstone interval at c. 40 m, in GGA01. The mudstone and the sandstone are the main lithologies surrounding the mine voids, hence, characterising their thermal properties and thermal response during heat injection and recovery has a key implication for the understanding of geothermal operations and heat storage applications. The comparison of the thermal signal recorded by the DTS cable at the depth of the clay relative to the mudstone and sandstone is used to investigate the effect of various borehole construction (e.g. different casing layers) and unconsolidated nature of this lithology (Fig. 1).

2.1.4. Thermal properties

The thermal properties for the coal, mudstone and sandstone were obtained from representative sub-cores sampled from GGC01, a 200 m deep borehole situated 1.4 km to the northwest of GGA01 (Monaghan et al., 2021), which might slightly differ from the lithologies intersected by GGA01. The samples were analysed using Modified Transient Plane Source Method at 20°C at both 'air dry' and fully saturated conditions. When not available from direct measurements, typical thermal conductivity, density and specific heat capacity values for the lithologies present in GGA01 (e.g. made ground, clay, gravel, sand), and for the borehole materials were taken from the literature (e.g. Gale, 2004; Dalla Santa et al., 2017; Waples and Waples, 2004; Robertson, 1988). These are compiled in Table 1 together with the saturated thermal conductivity, specific heat capacity and density values determined from the GGC01 samples.

The lithological succession was divided into eleven intervals based on the analysis of the GGA01 geological summary log (Monaghan et al., 2020). This simplified vertical discretisation of the lithostratigraphy was used as a basis for the description of the temperature profiles and the development of the 2D numerical model, to ensure a reasonable numerical computational time whilst accounting for the major changes in lithology with depth (see Section 2.3). For each interval, the average thermal conductivity λ_m, density ρ_m and specific heat capacity c_m were calculated using Eq. 1.

$$\begin{cases} \lambda_m = \sum \%_r \lambda_r \\ \rho_m = \sum \%_r \rho_r \\ c_m = \sum \%_r c_r \end{cases} \quad (1)$$

Where $\%_r$ is the relative proportion of rock types in the interval, as reported in the GGA01 chippings log, and λ_r, ρ_r and c_r are the saturated thermal conductivity, density and specific heat capacity values of each corresponding lithology in the considered interval. These are reported in Table 1 together with the calculated weighted mean thermal conductivity (λ_m), density (ρ_m) and heat capacity (c_m) for each interval.

2.2. Data acquisition and processing from the injection-abstraction experiment

The heat injection experiment was conducted between the 12th of September 2023 at 11:00 and the 29th of September 2023 at 14:00, followed by a one-week recovery period (until the 6th October 2023). Mine water with a temperature of c. 11.9°C was pumped from the GU mine workings via GGA07 at a rate of 12 l/s, and re-injected at the same flow rate into the GU mine workings via GGA01 (injection main at c 0.15 m) at a temperature of c. 17.4°C after its passage across the heat exchanger-heat pump system. The temperature was continuously monitored during both the heat injection and recovery periods (from the 29th of September to the 6th October 2023) via a wellhead sensor, a data logger installed at 22.7 m in GGA01 and by the FO-DTS cable configured in passive mode. In this configuration, a DTS interrogator box connected to the top of the FO cable generates a pulsed laser signal that propagates through the cable. The cable then acts as series of distributed temperature sensors and records the temperature-dependent backscattered signals. The interaction of laser light with the silica core of the FO cable and time domain reflectometry principles are then used to calculate the temperature of the cable at discrete sections of the fibre (McDaniel et al., 2018). This allows recording the temperature changes resulting from heat transfers in the subsurface in response to the heat injection in GGA01. During the heat injection and recovery test, DTS recorded the temperature change every 10 min along the full borehole length at a 25 cm resolution.

Table 1
Thermal properties for (a) the GGA01 lithological succession and (b) the borehole materials. The thermal conductivity, specific heat capacity and density for each lithological interval (λ_m, c_m and ρ_m) corresponds to the average of the rock type property values ($\lambda_{r,sat}$, c_r, and ρ_r) weighted to the proportion of rock type within the interval ($\%_r$). The water properties are indicative and temperature-dependent variables.

a) Lithologies		Made ground	Sand	Gravel	Clay	Sandstone	Mudstone	Coal	Weighted average		
λ_{rsat} (W/(m·K))		5.03 [a]	2.0[b]	2.4[b]	1.11[b,f]	3.49[d]	2.42[d]	0.68[d]			
c_r (J/(kg·K))		1270 [a]	1632[a]	1175[a]	860[c]	775[c]	930[e]	1300[c]			
ρ_r (kg/m^3)		2182 [a]	2010[a]	1983[a]	2680[c]	2520[d]	2130[d]	1290[d]			
Min depth (m)	Max depth (m)	$\%_r$							λ_m	c_m	ρ_m
0	8.3	100 %							5.03	1270	2182
8.3	16	100 %							5.03	1270	2182
16	19		50 %	5 %	45 %				1.62	1262	2310
19	22			10 %	90 %				1.23	892	2610
22	26		45 %	50 %	5 %				2.16	1365	2030
26	29.5					100 %			3.49	775	2520
29.5	29.7					70 %		30 %	2.65	933	2151
29.7	30.5					20 %	70 %	10 %	2.46	936	2124
30.5	47.5					96 %	0.3 %	4.1 %	3.38	795	2473
47.5	48.9					36 %	12 %	52.4 %	1.90	1067	1834
48.9	52					4 %	96 %		2.46	924	2146

b) Borehole material	Thermal conductivity λ_{bh} (W/(m.K))	Specific heat capacity c_{bh} (J/(kg K))	Density ρ_{bh} (kg/m^3)
Water @20°C	0.64	4184	1000
Grout	1.3[d]	1500[d]	1800[d]
Boode PVC casing	0.17 [g]	880 [g]	1400 [g]
Steel casing	40 [g]	475 [g]	7850 [g]
Rubber	0.5 [g]	1900 [g]	1100 [g]

Sources:
[a] Hamdhan and Clarke (2010)
[b] VDI 4640 (Dalla Santa et al., 2017)
[c] Waples and Waples (2004)
[d] Unpublished GGC01 borehole rock sample data
[e] (Robertson, 1988)
[f] Gale, (2004)
[g] COMSOL Multiphysic default values.

Following the experiment, the raw DTS data previously calibrated were compiled and converted into a usable two-dimensional section representing the variations of the temperature with depth and with time. This conversion process involved correcting the depth values for the length-along-fibre (LAF) representing the distance between the DTS monitoring box and the borehole top. The top 2 m of the DTS profile were subsequently erased to withdraw from the analysis the near-surface temperature, that is mainly controlled by the daily variations in air temperature and does not provide any useful information on the heat flow induced by heat injection at the depths of interest during the experiments.

Two types of datasets were extracted from the corrected DTS profiles. Temperature-depth profiles were selected to highlight the variation of the temperature with depth at key time steps during the pre-experiment period, the heat abstraction period and the recovery period. Representative temperature time-series were chosen to characterise the rate of temperature change at the depth of key lithologies in GGA01 (Fig. 1): a clay dominated interval (20.4 m depth), a mudstone dominated interval (30.5 m depth) and a sandstone interval (40.2 m depth). These time-series were used as a reference for the subsequent numerical modelling analysis (Table 2). Additional temperature time series at the depth of the made ground and GU mine working were analysed for comparative purpose. Those were not included in the numerical analysis, due to the poor constraints on the made ground properties and the complex nature of the hydraulic and thermal processes at the depth of the GU mine workings, that are beyond the scope of this study.

2.3. Numerical modelling

2.3.1. Model design

1D horizontal axisymmetric numerical models accounting for the GGA01 borehole construction were developed using COMSOL Multiphysics® v. 6.2 (COMSOL, 2023) to investigate the effect of the borehole material and subsurface properties on the immediate and longer-term thermal response to heat injection recorded by the FO-DTS cable in the overlying rock mass.

Fig. 2a shows the borehole construction at the depth of the Quaternary deposits (between 17 m and 29.7 depth) and the boundary conditions for the 'clay model' that were implemented to best represent the conditions during the experiment. Within this interval, the borehole consists of two grout layers injected in the annulus between the PVC Boode and the steel casing (between r = 140 mm and r = 213 mm), and between the steel casing and the reservoir (between r = 229 mm and r = 280 mm), with r representing the distance from the model axis, i.e. borehole centre. The PVC Boode and the steel casing have 16 mm thickness.

Fig. 2b shows the representative model for the deeper section of the borehole that was used to evaluate the temperature response at 30.5 m (i.e. 'mudstone model') and 40.2 m depth (i.e. 'sandstone model'). In this section, only one grout layer (between r = 140 mm and r = 213 mm) is present to maintain the inner 16 mm-thick PVC casing. In all the numerical models, a distance of r = 141 mm was considered as the observation point (i.e. modelling output), representing the FO cable location.

Heat injection and thermal recovery were simulated in the same model as two sequential transient simulations for a duration of 17 and 14 days, respectively, with maximum time steps of 0.02 days. The models calculated the temperature change along the x-axis due to the radial transfer of heat between the borehole water and the surrounding rock mass during both heat injection and recovery, assuming heat conduction only (Eq. 2).

$$\rho_m c_m \frac{\partial T}{\partial t} = \mathrm{div}(\lambda_m \nabla T) \quad (2)$$

Where T is the temperature [K], and ρ_m, c_m and λ_m the density [kg/m^3], specific heat capacity [J/(kg·K)], and thermal conductivity [W/(m·K)] of the modelled material (Table 2).

The initial temperature distribution T_0 along the model axis was defined using the pre-experiment DTS value measured at the depth of the considered lithology in GGA01 and GGA02, situated 10 m apart (Table 2). Heat injection was expressed as a time-varying temperature boundary condition T_i along a line representing the water-filled borehole section of the model, using the temperature measured by the downhole logger installed in GGA01 during injection. A natural, or Neumann (i.e. no flow; $-n \cdot q = 0$) boundary condition was applied on the right side of the model. This boundary was placed far enough (r = 10 m) to avoid boundary effects. For the recovery simulation, the initial temperatures were those calculated at the end of the injection period. Both the water-filled section and the right side of the model were imposed a Neumann (i.e. no flow) boundary condition, allowing the system to slowly re-equilibrate based on the far field rock mass temperature.

2.3.2. Parameter evaluation and best-fit model

The representative 1D axisymmetric model that accounts for the borehole construction below 29.7 m depth (i.e. a single PVC casing) was used first to conduct a parametric analysis for the rock mass, grout and PVC casing thermal properties through a series of forward simulations. For each parameter, the minimum, step increase and maximum values were defined to include a range of representative values for the different material properties (Table 2). The subsurface properties for the base model were attributed the weighted average thermal conductivity, density and specific heat capacity values calculated in section 2.1.4. for the mudstone interval (Table 1). Due to the absence of direct measurements for the Glasgow Observatory boreholes, the borehole material

Table 2
Properties for the clay, mudstone and sandstone base models and range of values for the parameter evaluation. λ, ρ and c are the thermal conductivity, density and specific heat capacity, respectively. Subscripts m, c, s, and g refer to the rock mass, PVC casing, steel casing and grout, respectively. $T_0(x)$ is the estimated initial temperature distribution at the corresponding DTS observation depth z.

Property	Clay (Base)	Mudstone (Base)	Sandstone (Base)	Sensitivity Analysis		
				Minimum	Step	Maximum
z (m)	20.4	30.5	40.2			
$T_0(x)$ (°C)	11.9 - 0.03x	12 - 0.03x	12.1 - 0.03x			
λ_m [W/(m·K)]	1.23	2.46	3.38	1.0	0.5	4.0
ρ_m [kg/m^3]	2610	2146	2473	1500	500	3000
c_m [J/(kg·K)]	892	924	795	880	50	980
λ_c [W/(m·K)]	0.17	0.17	0.17	0.12	0.05	0.22
ρ_c [kg/m^3]	1400	1400	1400	-	-	-
c_c [J/(kg·K)]	880	880	880	-	-	-
λ_g [W/(m·K)]	1.3	1.3	1.3	0.8	0.5	1.8
ρ_g [kg/m^3]	1800	1800	1800	-	-	-
c_g [J/(kg·K)]	1500	1500	1500	-	-	-
λ_s [W/(m·K)]	40	-	-	-	-	-

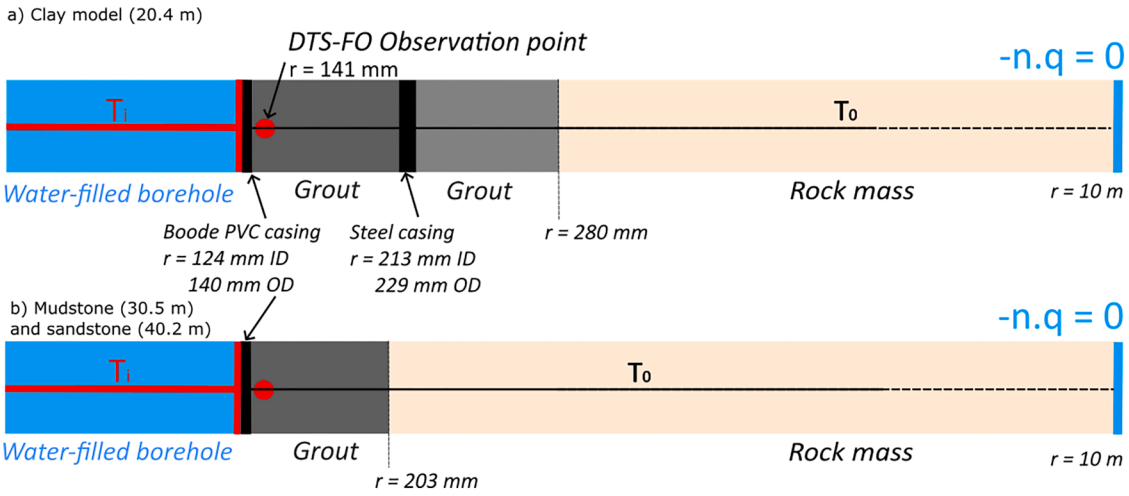

Fig. 2. 1D axisymmetric model geometry and boundary conditions a) for the clay (20.4 m) and b) for the mudstone (30.5 m) and sandstone (40.2 m) models. T_0 is the initial temperature distribution at a distance r from the model axis, T_i is the injection temperature imposed in the water-filled section of the borehole to the left side of the Boode PVC casing during heat injection. No flow (-n.q = 0) is applied on the right boundary during injection and recovery.

properties (e.g. thermal conductivity for the casing and grout) were defined according to representative values reported in the literature (COMSOL, 2023). Each evaluated parameter was modified individually, keeping the other borehole materials and rock properties constant. The thermal response at the location of the FO-DTS cable (r = 0.141 m) during both the heat injection and recovery for each scenario was compared with the DTS data (i.e. DTS at the mudstone interval) to understand the key parameters having a control on the thermal response recorded by the FO-DTS cable over the short and longer experiment time scale.

Models that best replicated the observed DTS response in the clay, mudstone and sandstone intervals (i.e. at 20.4 m, 30.5 m and 40.2 m, respectively) were finally developed through manual calibration of the base model properties for the corresponding interval (Table 2), using the appropriate borehole construction (Fig. 2). The best fit models were used to evaluate the combined effect of the borehole construction and lithology.

2.3.3. *Two-dimensional analysis*

A 2D axisymmetric model of the GGA01 borehole was then developed to investigate the 3D effects of heat transfers on the temperature distribution along a vertical profile, accounting for both the borehole construction and the lithological succession, i.e., the heterogeneities between the different sedimentary layers (Fig. 3).

The model consists of a 52 m deep and 10 m wide section composed of 99,721 triangles and 12,282 edge elements, with minimum size of

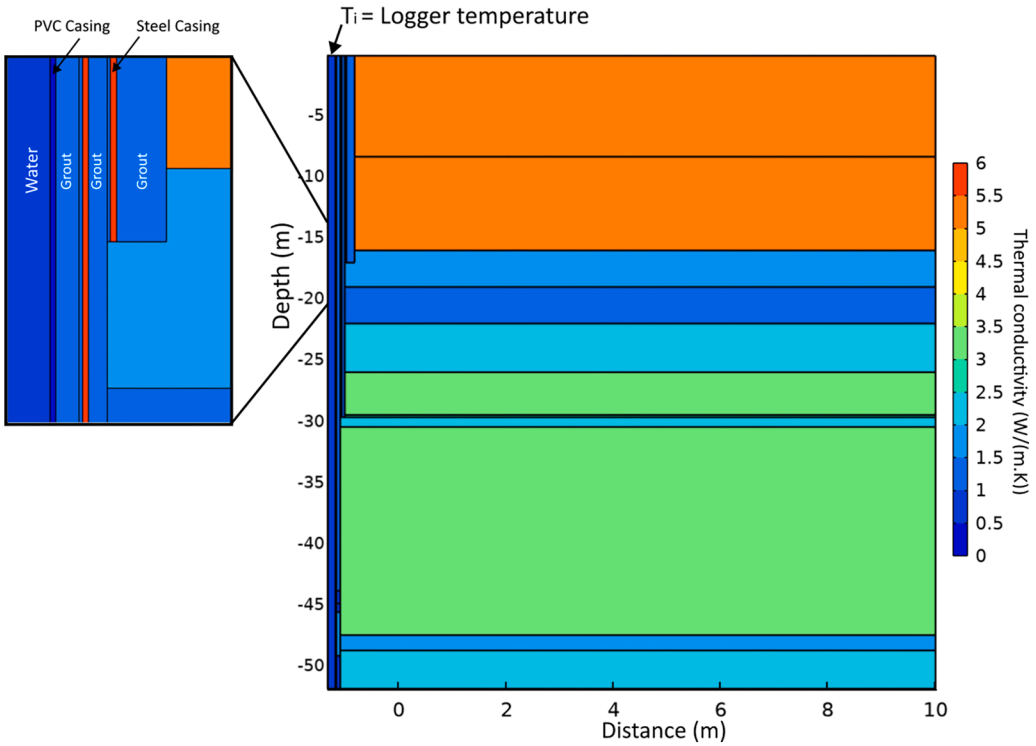

Fig. 3. Graphical representation of the 2D model configuration showing the thermal conductivity of each lithological interval and the borehole construction. T_i is the injection temperature (boundary condition).

0.01 m along the borehole/rock mass boundaries. The optimal mesh size was determined using a manual approach to ensure the independence of the results whilst optimising the computational time. The model was divided into eleven lithostratigraphic intervals, described in Section 2.1.4. Each interval was assumed to be homogeneous and was attributed the weighted average thermal conductivity, heat capacity and density calculated using Eq. 1 (Table 1a). Borehole materials were attributed typical values from the literature (Table 1b). Care was taken to ensure equivalence of the borehole material properties, subsurface properties and borehole construction between the 2D model and the 1D base models at the corresponding depth.

In the 2D reference model, an interpolation of the pre-experiment DTS depth profiles between boreholes GGA01 and GGA02, situated 10 m apart, was used to calculate the initial temperature distribution in the model, with the temperature at GGA02 representing the far-field temperature. Heat injection and recovery were simulated for a total period of 17 and 14 days, respectively, with maximum time steps of 0.1 days, assuming heat conduction only. The uniformity between the DTS and temperature logger installed below the injection main in GGA01 (see Fig. 1 and Section 3.1) indicates limited temperature variations within the borehole (Fig. 4). During injection, a Dirichlet boundary condition representing the temperature variations recorded by the logger (T_i) was therefore applied to the polygon representing the water-filled borehole (i.e. to the left side of the PVC casing). A groundwater velocity v of 0.005 m/s was set at the depth of the GU to represent the flow of mine water from GGA01, via the screened section of the borehole. This average linear velocity $v = \frac{Q}{A\varphi}$ was calculated using a volumetric flow rate Q = 0.012 m^3/s (abstraction/injection rate), a cross-sectional area $A = 2\pi rh$ = 4.6 m^2 (with h = 3.6 m the height of the screen section and r = 203 mm the internal borehole radius at the depth of the GU), and a porosity φ = 0.5. Neumann (i.e. no flow) boundary conditions were applied at the surface, bottom and right boundaries of the 2D model. During recovery, all boundaries were imposed a no-flow boundary condition. This allowed the system to return to an equilibrium via diffusive heat transfers, according to the temperature gradients normal to each boundary.

Subsequently, the 2D model was adjusted using a manual calibration approach and based on the learnings from the 1D model to improve the fit to the data. The best-fit properties were determined based on the combination of rock properties that best replicate the 1D vertical temperature profiles acquired by the FO-DTS cable in GGA01 at the end of heat injection (29th September 2023) and after one week of heat recovery (6th October 2023).

3. Results

3.1. Thermal response during the experiments

3.1.1. Temperature sensors

Fig. 4 shows the temperatures measured during the experiment in borehole GGA01 at wellhead (injection temperature) and the downhole logger (22.7 m depth). The temperature measured with the DTS cable at the screen interval (47.31 m depth) is shown for comparison.

The average injection temperature (wellhead temperature T) during the experiment was 17.4°C, with fluctuations between 16.7 and 17.9°C. At two times, 13th and 23rd September, two short problems with the heat pump decreased the injection temperature to 9.6 and 10.1°C, but this effect was limited to about 10 min. When the injection stopped, the wellhead logger was directly affected by ambient temperature. The wellhead data during the recovery period show the daily fluctuations at the surface.

The initial downhole logger temperature was 11.9°C. During the injection experiment, the measured temperatures were almost identical to those at the wellhead, including the rapid fluctuations, reflecting the location of the logger 7.5 m below the reinjection main. After the injection stopped, the temperature of the logger decreased gradually, to about 12.65°C the 6th of October, showing that the borehole water had not re-equilibrated completely to the initial baseline temperatures.

At the screened interval, temperatures measured by the DTS were slightly lower (c. 0.2°C) than the measured at wellhead. At this level the DTS cable is in contact with the injected water flowing through the slotted screen and the gravel pack. The lower temperatures might reflect heat losses due to transfer via conduction to the surrounding rock mass along the borehole walls. During recovery, the measured temperature decreased at a lower rate compared to the downhole logger, down to 14.55°C the 6th of October.

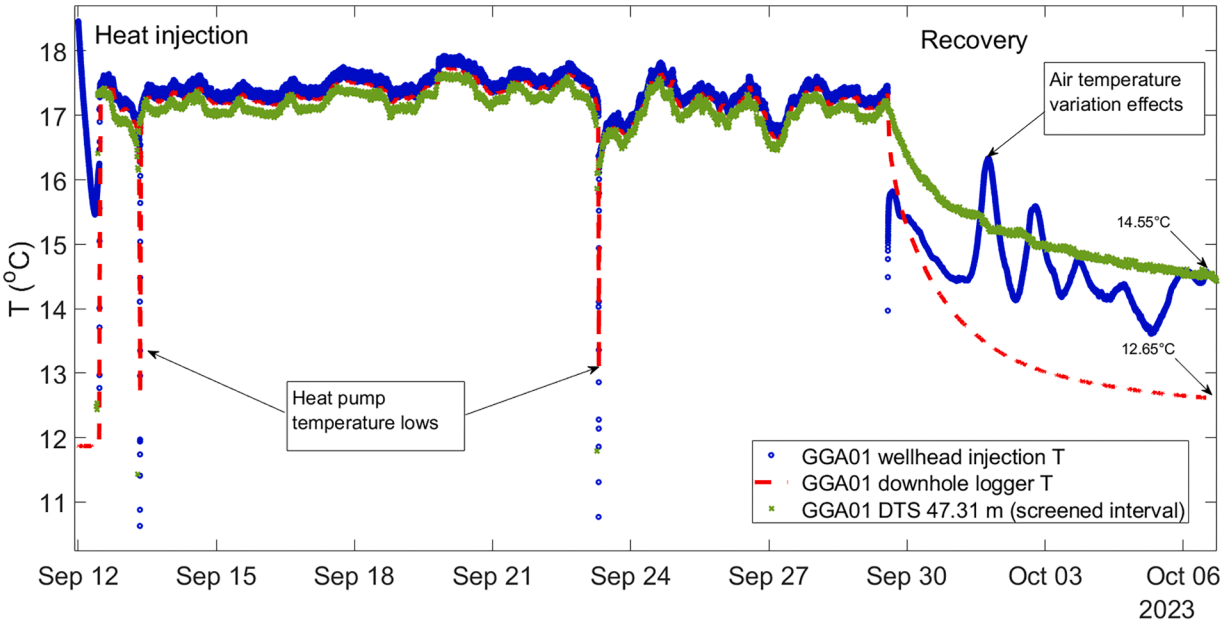

Fig. 4. Wellhead, logger and DTS temperatures measured in GGA01 during the heat injection (12/09/2023 - 29/09/2023) and the recovery period (29/09/2023 – 06/10/2023). Data suggests fluctuations in the injection temperature (at wellhead) between 16.7 and 17.9°C.

3.1.2. DTS

Fig. 5 shows the DTS data in GGA01 during the heat injection experiment and the subsequent thermal recovery period.

3.1.2.1. Injection. DTS recorded a continuous profile along the FO cable installed along the borehole over time. Fig. 5 shows that the temperature does not vary uniformly with depth. The initial (pre-injection) temperature profile (black line in Fig. 5d) showed a positive (downwards) geothermal gradient below the zone of seasonal influence (approx. 9 m depth) and down to the screened interval. The initial temperatures at the key intervals -clay, mudstone and sandstone- were 11.86°C, 11.95°C and 12.11°C, respectively. At the screened interval, the initial pre-

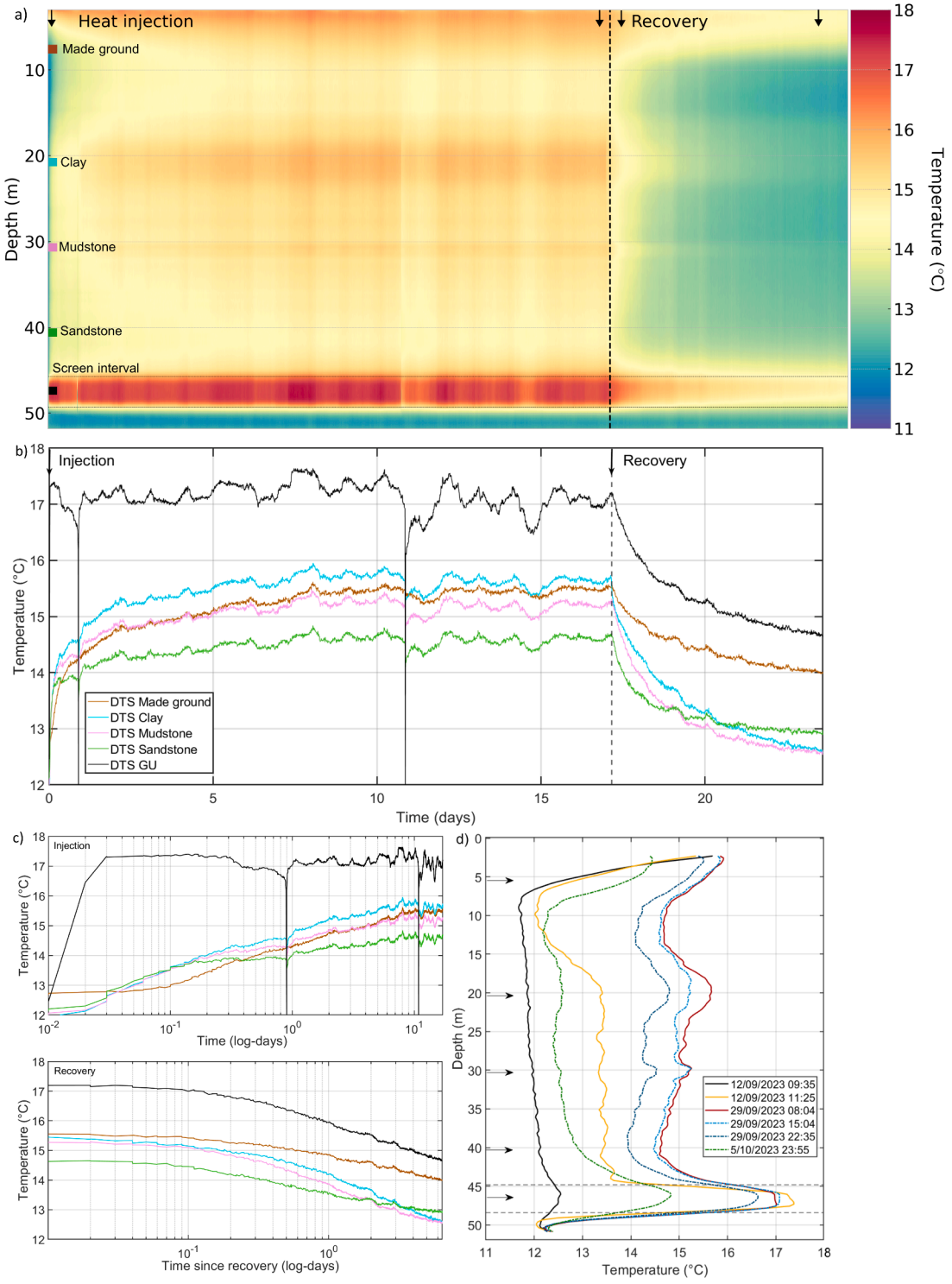

Fig. 5. a) DTS in GGA01 during heat injection and recovery (12/09/2023 to 6/10/2023). The coloured dots indicate the observation depths (panels b and c), and the vertical arrows the location of the temperature profiles (panel d). b) Temperature change at 5.4 m (made ground, dark red), 20.4 m (superficial clay deposits, light blue), 30.5 m (mudstone, magenta), 40.2 m (sandstone, green) and 47.5 m (Glasgow Upper mine workings, black). c) Temperature timeseries during injection (upper panel) and recovery (lower panel) in log scale. d) DTS profile acquired in GGA01 before the experiment, during heat injection and recovery. The arrows indicate the observation depths and the dashed line the depth of the screened interval (45.7 m – 49.3 m).

experimental temperature was the highest at 12.5°C.

Following the onset of heat injection, a rapid 4.6°C warming was observed between c. 46 m and 48 m depth. This interval corresponds to the depth of the slotted screen (45.7 m – 49.3 m), where the FO cable is in direct contact with the water injected in GGA01 as it flows towards the GU mine working. The temperatures measured at this interval reached the maximum values 45 min after the experiment started, but this large increase in temperature was initially constrained to the ~3.6 m of the screened section. Over time, the thermal anomaly around the GU tended to dissipate and spread upwards, as suggested by the progressive warming of the zone above the GU in the later heat injection profiles (Fig. 5d).

In the rest of the borehole, there was a progressive warming measured along the whole cased section. In general, the thermal profile tended to invert, with the positive gradient observed before the start of the experiment (black line in 5d), evolving towards a negative gradient at the end of the test (red line in 5d) with depth-dependent temperature variations related with the changes in lithology. More pronounced warming intervals were observed between c. 18–22 m depth (below the injection main) and at c. 30 m depth, which correspond to the depth of the clay and gravel interval and mudstone with minor coal layer, respectively. Less pronounced warming was observed in the made ground (shallower 8 m), superficial deposits between 8 – 16 m depth and sandstone interval (c. 40 m). In contrast to the slotted screened interval, there is no connection between the borehole water and the FO cable in the cased section between the surface and 45.7 m depth. Therefore, the thermal response to heat injection recorded by the FO cable above the screen is expected to result mainly from conductive heat transfers throughout the borehole walls and porous media.

Near the surface (i.e. above c. 6 m depth), a zone of higher temperature relative to the initial background temperature was observed both in the 2D and 1D temperature profiles (Fig. 5(a and d)). This c. 16°C anomaly is visible before the start of the period of analysis and expands downward as the temperature in the borehole increases during the heat injection phase. Longer term signals related to surface changes and seasonal variations in air temperature have been observed to propagate down to c. 8–9 m below the ground surface at the Observatory (https://www.ukgeos.ac.uk/glasgow/observatory-infrastructure/dts, Gonzalez Quiros et al., submitted). In Paisley, Glasgow, air temperatures of up to 20°C were measured in August 2023 (MetOffice, 2025), suggesting the potential control of surface temperature on the shallow temperature profile.

Temperature timeseries were extracted at various depths to evaluate the effect of key lithologies on the temporal changes and amplitude of the thermal response (Fig. 5(b and c)). Temperature changes at the screened interval that reflect the water injection temperature are also shown in the figure for reference.

At the three analysed lithologies and depths (clay, 20.4 m; mudstone, 30.5 m; and sandstone, 40.2 m depth) the temperature increased at a very similar rate by c. 1.8°C during the first c. 4 hours of the experiment. After 4 hours of injection (Fig. 5c with x-axis log scale for detail) the rate of temperature increase remained relatively high, but the three started to diverge until they reached their maximum temperatures after 8 days, with the maximum temperature observed for the clay (c. 15.95°C) and lower for the sandstone (c. 14.82°C). After 8 days, the temperatures started to stabilise reaching a quasi-steady state (with fluctuations reflecting the injected water temperatures) over the last 9 days of the test. At the end of the injection period, the temperature in the clay was 15.7°C and in the mudstone 15.32°C, 3.84°C and 3.37°C higher than the pre-experiment temperature respectively, whilst the temperature in the deeper sandstone interval was 14.66°C, only 2.46°C higher than the pre-experiment temperature.

In comparison, the data measured at the depth of the made ground (5.4 m depth) showed a very different evolution. The increase in temperature was slower, not starting to increase at a considerable rate until c. 1 hour after the start of the experiment (Fig. 5c). The made ground interval is situated above the injection main (15 m depth), where the borehole construction consists of three casings and grouted annulus (Fig. 1). The observed temperature is therefore likely to be more influenced by the borehole design and material properties to a depth of 17 m compared to the observations at greater depth. Temperatures at the made ground depth increased continuously with a very different rate when compared with the other depths, reaching a maximum temperature of 15.56°C after 8 days.

During injection, the variations in temperature observed at all depths (Fig. 5(b)) depicted a strong sensitivity to the variations in the injected water temperature (Fig. 4). The maximum measured temperature in all the identified locations coincides with the maximum injection temperature registered the 20th September (8 days after starting the injection). The amplitude of the changes measured in the cased parts are however lower and smoothed (especially for the made ground with three casings) compared with the injected water temperature. For example, the fluctuation of 0.8°C in the injected water temperature the 27th September, produced a change of 0.3°C in the clay, mudstone and sandstone, and a variation of 0.1°C in the made ground.

3.1.2.2. Recovery. The period of thermal recovery considered in this work corresponds to the period covering the progressive return to equilibrium temperatures following the cessation of the heat injection on the 29th September 2023 until the experiment was considered finished on the 6th October 2023. The temperature timeseries in Fig. 5 (b,c) show the rate of temperature change during recovery for the same key lithologies and depths analysed for the injection period.

The temporal evolution after the injection ended was very different for all the levels analysed. The clay interval showed the largest temperature drawdown, from an initial temperature of 15.7°C at the start of the recovery, to 12.65°C after 6 days, while the initial recovery temperature at the mudstone was 15.32°C and it reached 12.6°C after six days of recovery. These are temperatures still 0.79°C and 0.65°C higher than the pre-injection temperatures. The sandstone showed a very different trend, starting 14.66°C and reaching 12.95°C after 6 days, 0.84°C lower than the pre-experiment temperature at that level. The made ground depicted the slowest rate of return at the initial times, as shown for the heating part during the injection, which contrasts with the observations in the other intervals. However, after c. 2 days the rate of temperature change increased. After six days of recovery, a temperature of 14°C was measured at the depth of the made ground, which was 1.33°C higher than the temperature measured before the start of the experiment.

The largest residual thermal disturbances were observed at the depth of the GU mine working. There, the FO cable is in contact with the mine water that circulates in the open voids and therefore is the result of a combination of heat transfer processes. At that interval, the temperature during recovery varied from 17.15°C measured at the end of the injection down to 14.74°C six days after the injection stopped, still 2.24°C higher than pre-injection temperature at this interval.

The average temperature along the DTS profile after 6 days of recovery (green line in Fig. 5d), was about 0.5–0.8°C higher than the initial pre-experiment temperature, and up to 2.24°C higher in the GU interval. Depth temperature profiles suggest a progressive diffusion of heat (i.e. via conductive heat transfers) above and below the GU mine working during the heat injection phase, that becomes more prominent during the recovery phase (Fig. 5(a and d)). As the temperature declined, the heat dissipated upwards (i.e. up to 40 m depth), leading to a smoother thermal anomaly around the GU depth, and suggesting the prominence of vertical heat transfers during recovery.

The differences between the pre-experiment temperatures and those measured at the end of the experiment suggest that recovery was not completed within the period included in the analysis, with the largest disturbances being observed at shallow depth and in and around the screened interval.

3.2. Modelling results

Numerical modelling was performed to characterise the key controls on the rate of temperature change during heat injection and recovery, by determining the key properties (e.g., relative effect of heat conductivity vs groundwater flow) and processes (e.g., heat conduction vs heat convection) that best replicate the DTS observation at the depth of key lithologies encountered by GGA01.

3.2.1. Parameter evaluation

Fig. 6 shows the modelled temperatures for a range of thermal properties at the location of the FO-DTS cable (r = 0.141 m), alongside the DTS observations at 30.5 m depth (i.e. mudstone interval), displayed for comparison.

3.3. Rock thermal conductivity

The results presented in Fig. 6a show that the modelled temperature is highly sensitive to the rock thermal conductivity (λ_r). Higher λ_r reduce the rate of temperature increase, and at any given time, the higher λ_r and the lower the observed temperature. The log-scale analysis suggests that the temperature becomes sensitive to the subsurface properties after c. 2.5 h of injection (i.e. where the curves split for different thermal conductivity values). At the end of the injection period, a minimum temperature of c. 15°C is calculated for λ_r = 4 – 4.5 W/(m·K) and a maximum of 16°C is calculated for λ_r = 1 W/(m·K).

The thermal recovery rate after the cessation of heat injection also highly depends on λ_r. High λ_r results in a relatively fast return to equilibrium, which is expressed by a larger temperature decline at the start of the recovery period, which also largely relates to lower temperature observed for high λ_r at the start of the recovery period. At the end of the modelled recovery period, the higher λ_r and the lower the temperature, with a minimum temperature of 12.3°C observed for λ_r = 4 – 4.5 W/(m·K) and a maximum of 12.8°C observed for λ_r = 1 W/(m·K). This suggests that λ_r has determinant control on the long-term thermal recovery rate and the thermal disturbances induced by heat injection. It is however important to note that the relationship between the thermal conductivity and the observed temperature is non linear, and that the recovery rate and time to reach equilibrium is increasingly sensitive to a change in λ_r within the lower end of the range of λ_r values tested.

3.4. Rock heat capacity and density

The temperature was calculated for multiple combinations of independent rock density and heat capacity values using a multiparameter sweep. Due to the negligible sensitivity of the temperature to the rock density, Fig. 6b only shows the results for the combination of the minimum and maximum ρ_r and c_r for the range of values tested (Table 2). As

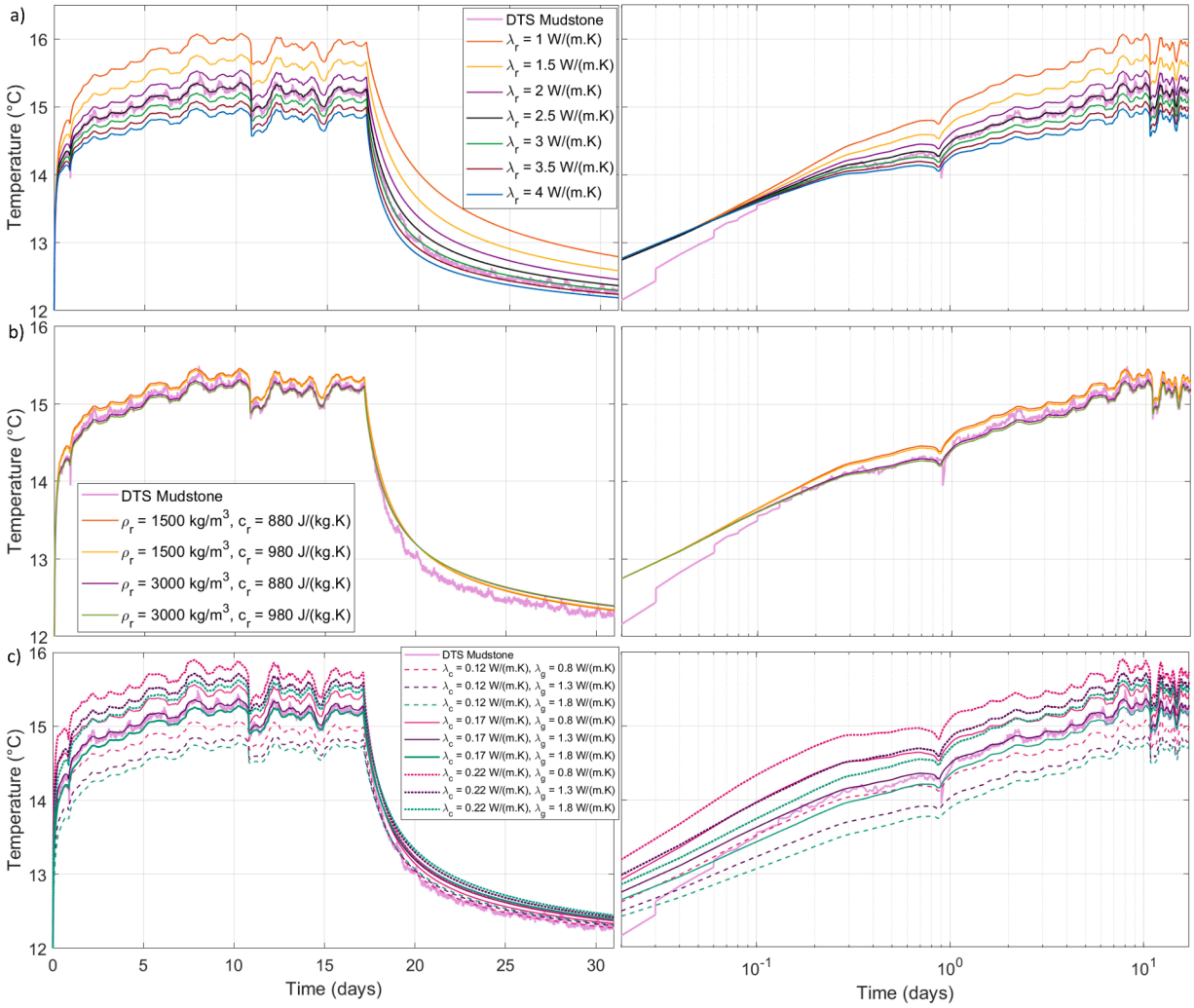

Fig. 6. Parameter evaluation on a) the rock mass thermal conductivity (λ_r), b) the density (ρ_r) and specific heat capacity (ρ_c) and c) the grout (λ_g) and casing (λ_c) thermal conductivity. The light purple line represents the measured temperature change at 29.5 m (mudstone). The other constant base model properties are summarised in Table 2.

for the rock thermal conductivity, the temperature becomes sensitive to the density and heat capacity of the rock mass after c. 2.5 h of heat injection. During injection, the higher ρ_r and c_r, the lower the rate of temperature increase and the lower the observed temperature at a given time. However, the temperature difference at the end of the injection period reached a maximum of 0.2°C for a difference in density of 1500 kg/m^3. After c. 3 days of recovery, the temperature returns to a smilar value for all density and heat capacity combinations, suggesting that those properties had negligible impact on the thermal recovery rate and long-term thermal near-borehole state, for the test conducted.

3.5. PVC casing and grout thermal conductivity

The casing and grout thermal conductivity both have a strong effect on the short-term thermal response to heat injection (Fig. 6c). The rate of temperature increase in the initial hours of heat injection is mostly dependent on λ_c, with a higher λ_c leading to a faster and larger temperature increase. This effect is more pronounced in scenarios with low λ_g. Low λ_g values result in a strong temperature increase at the start followed by a decrease in the rate of temperature change (i.e. pink dotted curve). If the λ_g is high, the rate of temperature change is lower and relatively constant thoughout the first part of the injection period (i.e. green dotted curve), i.e. until the properties of the rock mass become the dominant control. This leads the curves to converge for high λ_c. In adition, the higher λ_c and the lower λ_g, the greater the sensitivity of the thermal response to the variations in the injected water temperature. After one day of heat injection, the rate of temperature change becomes relatively similar for scenarios with $\lambda_g \geq 1.3$ W/(m·K) . A temperature difference of up to 1°C observed at the end of the heat injection period for difference in λ_c of 0.1 W/(m·K).

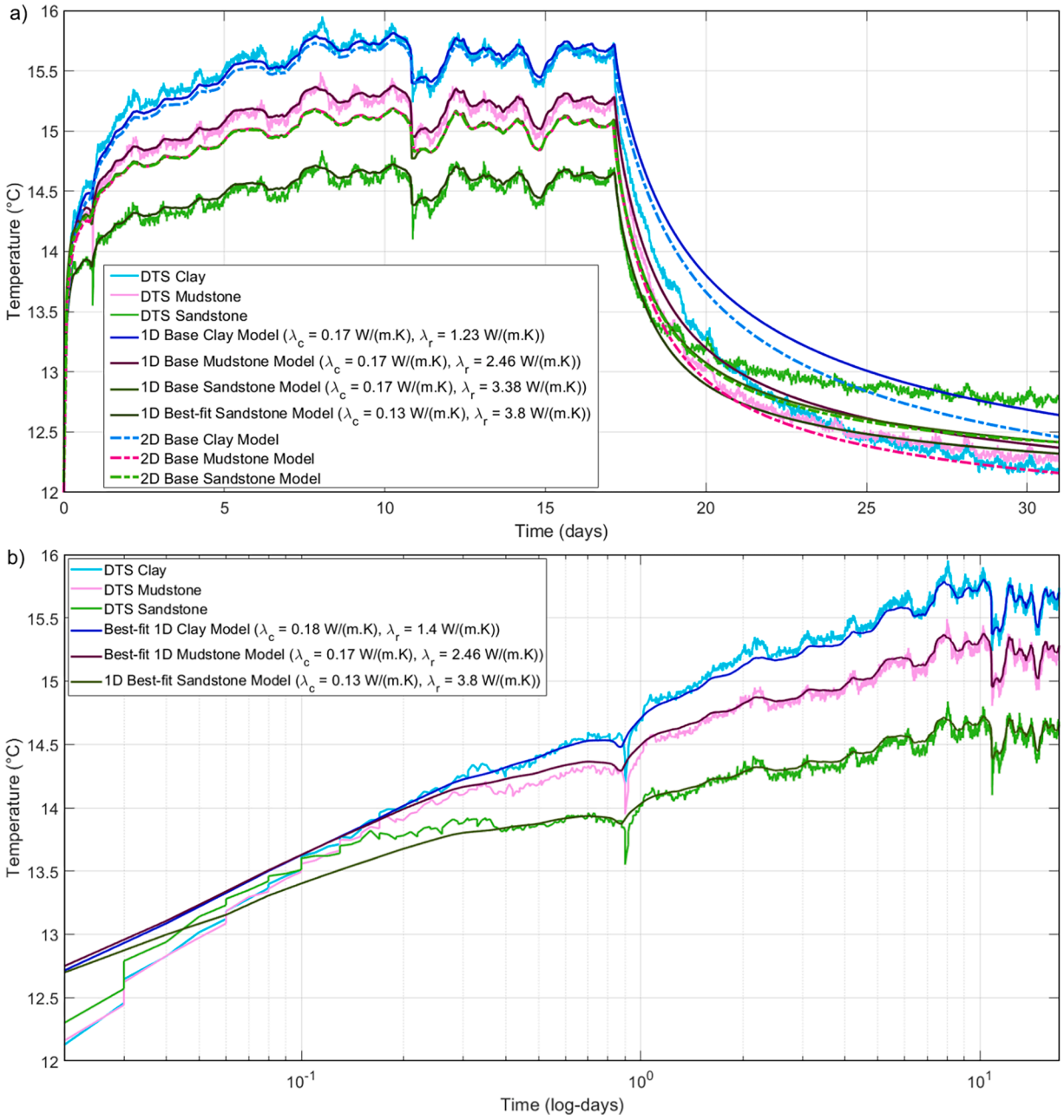

Fig. 7. Comparison of the modelled and observed DTS at the depth of the clay (20.2 m), mudstone (30.5 m) and sandstone (40.4 m) intervals for the 1D model and 2D models. The top graph displays the temperature variations during both injection and thermal recovery in cartesian scale for the 1D and 2D base models. The bottom graph represents the temperature variations during heat injection only on a logarithmic scale for the best fit 1D models.

During recovery, the effect of grout conductivity is negligible and the casing conductivity only slightly affects the rate of temperature change. At the end of the recovery period, a temperature difference of 0.2°C is observed for a 0.1 W/(m·K) difference in λ_c.

3.5.1. Base and best fit models

A refined analysis was conducted to identify the combination of borehole and rock properties that best replicate the DTS observations at the depth of the clay, mudstone and sandstone intervals. For each model, the base model properties were attributed according to the values reported in Table 2 and manually adjusted to improve the fit to the data over the different time periods of heat injection and recovery, using a trial-and-error approach. The modelling results for the base and best-fit models presented in Fig. 7 are compared to the DTS observations at 20.4 m (clay), 30.5 m (mudstone) and 40.2 m depth (sandstone).

The results suggests that the assumed λ_c and calculated λ_m for the 1D mudstone base model allow to best replicate the observations at 30.5 m for most of the injection period, with $\lambda_c = 0.17$ W/(m·K) and $\lambda_r = 2.46$ W/(m·K). The discrepancies are higher for the 1D clay and sandstone models. Whilst the base model parameters for the clay (i.e. $\lambda_c = 0.17$ W/(m·K) and $\lambda_r = 1.23$ W/(m·K)) best replicate the observations after c. 6 days, a model that best fits the DTS data in the early days of heat injection, shown on Fig. 7b, is found for $\lambda_c = 0.18$ W/(m·K) and $\lambda_r = 1.4$ W/(m·K). In the sandstone base model, the casing thermal conductivity $\lambda_c = 0.17$ W/(m·K) highly overestimates the temperature increase due to heat injection, and the best-fit temperature is obtained for $\lambda_c = 0.13$ W/(m·K) and $\lambda_r = 3.8$ W/(m·K), which is slightly higher than the base value calculated for the sandstone interval, despite a relatively poorer match to the data over the first c. 10 hours of the experiment (Fig. 7b).

For all 1D models, the modelled temperature during recovery poorly fitted the DTS data. For both the 1D mudstone and the clay models, all scenarios tested during the analysis underestimated the rate and amplitude of the thermal drawdown despite a relatively good fit to the data during injection. For the 1D sandstone model, all scenarios overestimated the amplitude of the thermal drawdown, suggesting that other controls are implicated in the return to an equilibrium. This is discussed further in section 4.

3.5.2. Axisymmetric model

3.5.2.1. Temperature profiles. The 2D axisymmetric model allows characterising the effect of lithological variations and the associated heat transfer processes observed on the measured downhole DTS profiles (Fig. 5d). The calculated temperature profiles (Fig. 8) suggest a relatively good fit between the modelled temperature at the end of the injection period and the DTS data below the made ground (at c. 16 m) and above the sandstone interval (at c. 32 m). Only minor discrepancies between the 2D abstraction model (light blue dashed profile) and the data (light green profile) can be attributed to the simplified vertical discretisation of the lithostratigraphic succession in the model (i.e. not a detailed consideration of the variation in lithologies within each layer). A good fit is also observed at the depth of the GU mine working, although the warming of 17.4°C is modelled across the depth of the gravel pack/screened interval (between 46 m and 50 m), whilst it is concentrated in the upper part of the screened interval (between c. 46 and 48 m) in the DTS data. Larger discrepancies are observed in the made ground and superficial deposits intervals (above 16 m), where limited information on the nature of the deposits is available. In the lower part of the sandstone interval (between 35 m and 44 m), the model overestimates the temperature increase induced by heat injection. The potential cause for this (e.g. effect of grout thickness, see dark green dashed profile) is discussed in Section 4.2.

The modelled profile after one week of recovery (dark blue dashed profile) shows a relatively good fit with the DTS data (yellow profile) in the made ground, where the temperature highly depends on the long-term surface temperature signal. Below the made ground (c. 8 m) and down to the bottom grout (c. 44 m), the modelled temperatures are in average 0.4°C lower than the data, suggesting that the model overestimates the thermal recovery rate. However, both the observed and modelled temperature profiles depict a similar gradient. These discrepancies are lower in the clay-dominated interval of the Paisley Clay Member (19 – 22 m), where the difference between the model and the

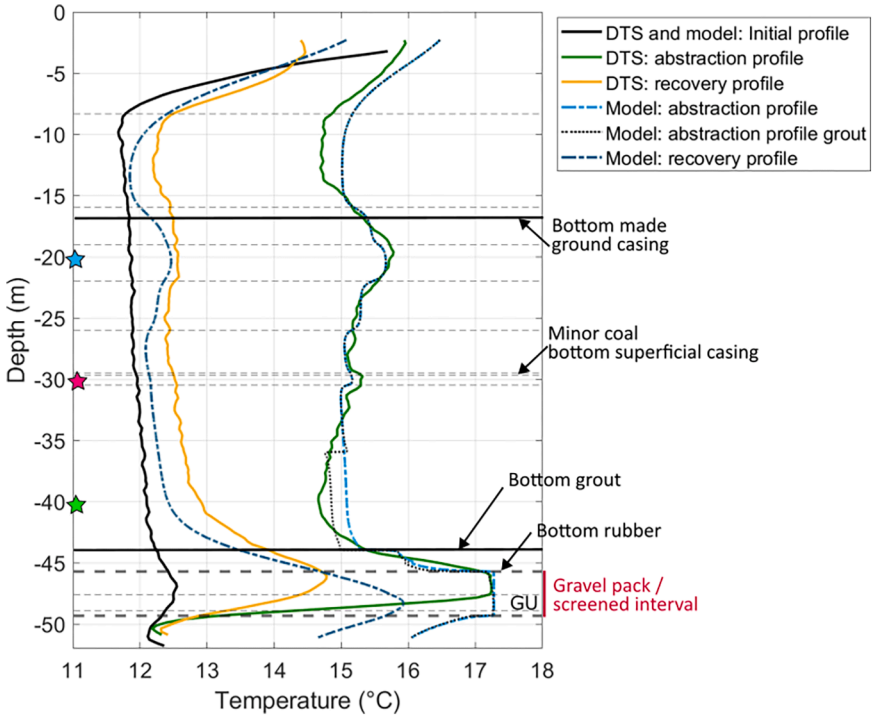

Fig. 8. Modelled and measured DTS profiles at the end of the heat injection and recovery periods (2D model). The horizontal dashed line represents the lithological intervals. The black dotted profile shows the results for a model with reduced grout thickness between 35 m and 44 m (see Section 4.2).

data is only c. 0.1°C. At the depth of and above the GU, the temperature remains higher than the measured temperature at the end of the modelled recovery period. The temperature peaks at the depth of the GU, whilst it is the maximum at the top of the gravel pack in the DTS profile.

3.5.2.2. Temperature time series and vertical heat transfers. In the 2D base model results, the temperature change at the depth of the clay depicts a good fit to the DTS during injection. However, the modelled temperature at the depths of the mudstone and sandstone is similar throughout the injection period, underestimating the temperature at the mudstone depth and overestimating the temperature at the sandstone depth, and diverge during recovery (Fig. 7a). Over both intervals, the borehole geometry is similar and the difference in the thermal conductivity of the rock mass is of c. 1 W/(m·K). These large discrepancies suggest potential differences between the actual borehole construction relative to the one reported (i.e. radius of the annulus and thickness of the grout layers, discussed in Section 4), inaccurate considerations of the vertical heterogeneities in the lithological succession or estimates of the key thermal properties (e.g., thermal conductivity).

3.5.2.3. and 2D comparison and vertical heat transfers. The time series extracted at 20.4 m, 30.5 m and 40.2 m in the 2D model were compared to results from the corresponding 1D base models for the clay, mudstone and sandstone, for which the thermal properties are well defined, but vertical heat transfers are not accounted for. In the sandstone base model, both 1D and 2D approaches provide similar results, with slight discrepancies observed after c. 11 days of injection (e.g. local temperature low) attributed to the higher time resolution of the 1D simulation (i.e. 0.02 days for the 1D approach and 0.1 days for the 2D approach). Discrepancies between the 1D mudstone and clay models and their corresponding time series in the 2D base model suggest the key effect of vertical heat transfers on the recorded temperature profile (Fig. 7). This effect is particularly visible in the mudstone time series, with the 2D model predicting a temperature up to c. 0.5°C lower than the 1D model. These discrepancies are observed across the depth of the mudstone interval (Fig. 8). As shown in Fig. 1, the mudstone consists of a thin layer (0.7 m), and the observation point in the 2D model is located right on the edge of the underlying interval (96 % sandstone) and only a few mm from the overlying layer (70 % sandstone and 30 % coal). This contrasts to the clay model, where the closest lithological boundary in the 2D model is c. 2 m away from the observation point and the 2D base model only slightly underestimates the temperature predicted by the 1D base model.

During recovery, the return to a thermal equilibrium is faster in the 1D clay and mudstone models (with $\lambda_m < 2.5$ W/(m·K)) and slower for the 1D sandstone model ($\lambda_m = 3.4$ W/(m·K)) relative to the temperature at the corresponding depths in the 2D model. Throughout the recovery period, the discrepancies between the modelled temperatures using the 1D and 2D approaches increase for the clay and mudstone models and reduce for the sandstone model. This suggests that the vertical heat transfers play a key role during thermal recovery and is highly controlled by the thermal conductivity of the lithologies encountered.

4. Discussion

4.1. Thermal effects observed at the DTS cable

The thermal response recorded by the FO-DTS cable from the onset of heat injection in the cased section has been mainly associated to the conduction of heat from the injected water through the borehole walls, casing(s) and grouted annulus towards the rock mass and varies with depth at a rate that depends on the temperature contrasts and material thermal properties.

The DTS observations at the depths of the clay, mudstone and sandstone suggest that the temperature variation becomes sensitive to the subsurface properties after c. 2.5 h of heat injection. This is expressed on the temperature timeseries displayed in a logarithmic scale (Fig. 5c) by a divergence between the different temperature curves. Before that, the trend is similar for all lithologies, suggesting that the thermal response recorded by the FO-DTS cable and the heat transfers are mainly influenced by the borehole construction and the location of the FO cable attached to the casing (close to the source). During recovery, the DTS observations moreover suggested that the return to an equilibrium significantly varies depending on the lithologies and is the fastest for the sandstone. At the depth of low conductivity lithologies, i.e. the clay and to a lower extent the mudstone, thermal drawdown is delayed, and no thermal equilibrium is reached as the end of the one-week recovery period, suggesting that those lithologies tend to retain heat much longer.

The numerical analysis suggests that the combination of casing, grout and borehole thermal conductivity play a key role in determining the amount of heat that might be transferred and stored within the reservoir and overlying rock mass. The casing and grout thermal conductivity influences the temperature change over the short term (for approximately 8 hours) but impacts the total amplitude of the temperature change in the long term. This is expected, as the excess heat of the borehole water first travels through 7–14 cm of casing before reaching the rock mass. An opposite relationship between the observed temperature and the grout or casing thermal conductivity is observed and interpreted to relate to the location of the observation point (i.e. the FO cable) relative to the casing and grout. The thermal conductivity, and to a lower extent the density and heat capacity of the rock mass are shown to mainly controls the rate of heat transfer over the mid- to long-term (i.e. from c. 2.5 h), in accordance with the data, where the temperature is mainly dependent on heat conduction through the surrounding porous media and on potential heat advection via groundwater flow (Simon et al., 2021). Conductive heat transfers are the largest in the high-conductivity sandstone interval, between 30 m and 44 m, where the ΔT is the lowest, reaching steady values of 23 W/m^2 after 17 days of heat injection at r = 141 mm (radius of the DTS observation point). The lowest rate of heat transfers is calculated in the Paisley Clay member at 19 – 22 m, where the ΔT is the largest, reaching values of 16 W/m^2 (Fig. 9).

The rock mass thermal conductivity is also shown to control the thermal recovery rate, by enhancing or inhibiting horizontal and vertical heat transfers (Table 3). At the start of the recovery, the return to equilibrium is the quickest in the high-conductivity sandstone layer, with a calculated heat flux of c. 14 W/m^2, against 10 W/m^2 in the Paisley Clay Member interval (Fig. 9). After 20 days, the thermal recovery rate significantly reduces in the higher conductivity layers as they reach a thermal equilibrium, whilst it is the highest in the low conductivity layers, showing the persistence of residual heat (Fig. 8). However, the poor fit to the data during recovery suggests the control of other processes, not modelled in this study, such as the effect of groundwater flow, free convection in the borehole or of disturbances of the background subsurface temperature due to previous experiments at the Observatory.

4.2. Effect of uncertainties on thermal response analysis

4.2.1. Uncertainties in material properties

One of the key limitations of the numerical model development is the lack of constraints on the material and rock properties, where no in situ measurements are available. The lack of constraints on the material properties leads to multiple combinations of rock, grout and casing thermal conductivity able replicate the DTS signal. This is exacerbated for the superficial clay deposit model that is built with an additional layer of grout and steel casing and whose lithological characteristics are poorly constrained.

A 2D model with simplified thermal properties provides a good

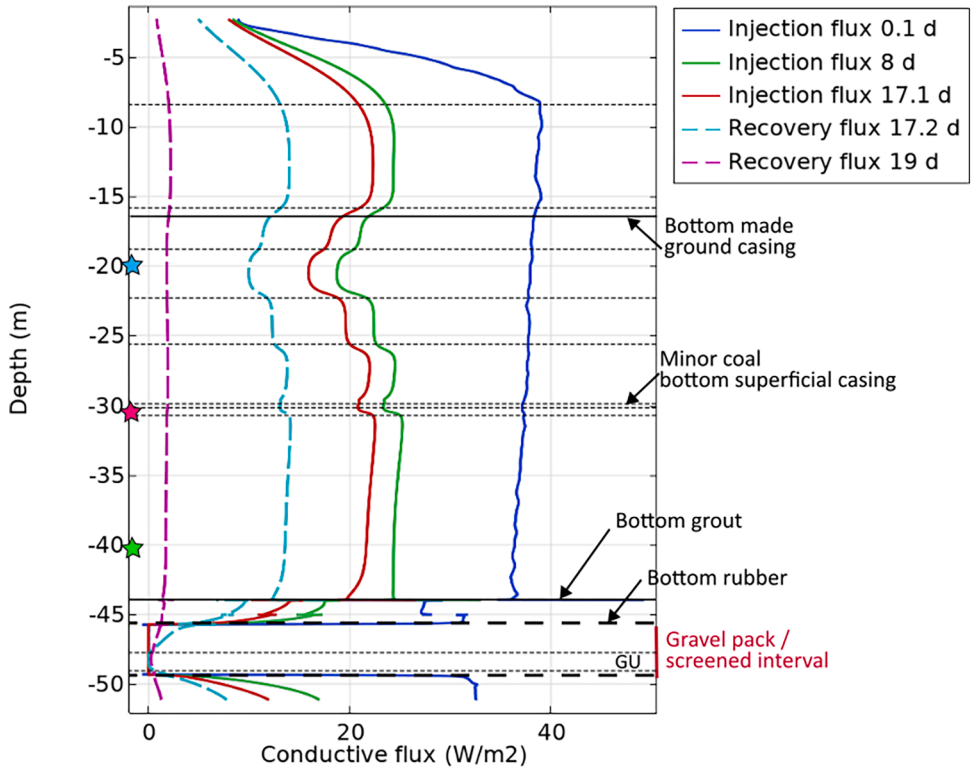

Fig. 9. Modelled conductive heat flux around GGA01(W/m^2) during heat injection and recovery, at r = 141 mm (DTS observation point).

Table 3
Summary of key parameters and heat transfer processes.

Process / Property	Transferable parameter
Thermal conductivity rock	Reduces rate of ΔT, increases rate of recovery
Heat capacity rock	Reduces rate of ΔT, negligible effect on recovery
Casing conductivity	Increase rate and amplitude of ΔT, limited effect on recovery
Grout conductivity	Reduces rate and amplitude of ΔT, limited effect on recovery
Vertical heat transfer	Effect on ΔT during injection, strong effect on recovery rate

approximation of the observed temperature changes at different depths and suggested the key control of vertical heat conduction. In the thin mudstone layer, a good fit in the 1D model using a thermal conductivity value of 2.46 W/(m.K) led to a 0.2°C discrepancy at the end of heat injection in the 2D model, highlighting the disturbances of the heat flux caused by high contrasts in the thermal conductivity between successive layers in heterogeneous systems (i.e. heat refraction effects, Majcin et al., 2012). Alternatively, it shows that accounting for vertical heat transfers (2D models) is essential to accurately estimate the thermal properties of lithologies in heterogeneous succession.

4.2.2. *Borehole construction*

As for the rock properties, there are no reports on the borehole materials characteristics at the Glasgow Observatory, leading to difficulties in constraining the best combination of borehole materials and rock properties. In this study, the models were developed based on the geometry reported in Monaghan et al. (2020). It is however suggested that differences in the borehole construction relative to the one reported might generate discrepancies between the observed and modelled temperature response. For example, the grout thickness might vary depending on the annulus space between the casing and the rock mass developed during drilling, depending on the rock competency. Grout losses might result from fracturing in brittle rock such as sandstone whilst impermeable lithologies prone to elastic deformation (e.g. shallow unconsolidated clay) might be associated to a smaller annulus space, reducing the grout volume around the FO cable. Depending on the rock properties (i.e. thermal conductivity contrasts between the grout and the rock mass), a thicker or thinner grout thickness can increase or decrease the predicted thermal conductivity in the near-borehole area. This would in turn modify the heat transfer rate and the temperature signal recorded by the FO-DTS cable within the first hours of heat injection. A model with reduced grout thickness in the bottom part of the sandstone interval (between 36 and 44 m) confirms that the grout thickness impacts the thermal response during heat injection and improves the fit to the DTS data (Fig. 8), and therefore the borehole construction may impact the performances of heat storage and recovery in the long-term.

4.2.3. *Hydraulic processes*

In addition to the effect of poorly constrained thermal boundaries mentioned above, it is suggested that hydraulic processes in the borehole (e.g., vertical free heat convection), the mine workings and overlying rock mass (e.g., heat advection) might need to be considered to explain the thermal recovery process. Discrepancies between the data and modelled temperatures at the depth of and above the GU at the end of the modelled recovery period moreover suggest that assuming a water dominant interval in the GU might not be appropriate. Attributing solid properties to the GU mine workings to account for heat conduction through porous material, in accordance with the presence of packed waste reported by Monaghan et al. (2021), might be necessary to best replicate the temperature within this interval.

In GGA01, the injection main is situated at c. 15 m in GGA01, at the transition between the superficial deposits (8 – 16 m depth) and the Paisley Clay Member interval (16 – 22 m depth). The injection of warm water at that depth might therefore be responsible for the strong warming at the depth of the clay interval, rather than being the expression of a low rock thermal conductivity and explain the poor fit in

the recovery profile. Above the injection main, the temperature might be lower than the one recorded by the logger, situated at c. 23 m depth, and explain the absence of extensive warming above c. 16 m.

4.3. Significance for mine water geothermal and heat storage

4.3.1. Geothermal characterisation

DTS was shown to be sensitive to contrasts in lithologies that strongly influence the rate of temperature change and the temperature distribution along the borehole. i.e. 0.86°C/d, 0.95°C/d and 1.02°C/d within the first 4 h of heat injection for the sandstone, mudstone and clay, respectively, and 0.33°C/d, 0.43°C/d and 0.51°C/d within the first 8 days and -0.28°C/d, -0.45°C/d and -0.48°C/d over the 6 first days of recovery. Thanks to the high temporal and spatial resolution of acquisition, DTS data collected during heat injection and interpreted using numerical modelling was demonstrated to have the potential to identify heterogeneities in the lithological succession, refine the characterisation of subsurface properties and therefore provide more accurate estimates of the geothermal resource. The key results are that clay and mudstone have a slower rate of heat transfer (i.e. larger accumulation of heat near the borehole with large ΔT and long return to equilibrium) and that sandstone has a smaller heat storage/recovery potential (i.e. low ΔT and quick return to equilibrium, with diffusion of heat further away from the borehole).

4.3.2. Relevance for storage

The monitoring of temperature change during the injection and recovery periods offers invaluable insights to study, understand and provide more accurate forecast of the long-term heating and recovery stages of different lithologies following heat injection/abstraction cycles in thermal energy storage applications.

In this study, the observations at the depth of the GU suggests that the heat progressively dissipates vertically from the mine workings, where the injected water dominantly flows. In that interval, the thermal recovery is slow relative to the borehole sections where the water is isolated from the mine working (i.e. -0.35°C/d) (Fig. 9), and this is attributed to the persistence of warmer injected water in the GU following the cessation of injection. The diffusion of heat (and/or advection in overlying fractured rock mass) up to c. 5 m above the screened interval after 1 week of recovery suggests that in a MTES setting, a larger amount of heat can be stored within a larger rock mass volume accessed by mine workings. Adding the extent of the mine itself to the specific surface of host bedrock would imply that the total reservoir volume is much larger than the considered volume of mine workings and galleries. Whilst assessment of the available heat and storage potential of mines are often limited to the volume of rock that has been mined out, this suggests that the volume of rock (i.e. including the fractures zone and further above) around the mine workings and galleries across the extent of the mine has key storage effects within a week of heat injection/recovery and needs to be accounting for in cyclical heat storage assessments. This is in agreement with the findings from Guo et al. (2018), who highlighted using numerical modelling that the height of the fractured zone, that depends on the strength of the rock mass overlying the mine roof, has a key effect on the heat extraction rate from flooded mine workings.

The collected data has shown the effect of conduction on nearby lithologies and how the affected volume is not restricted to the flooded mine voids. Therefore, the results presented in this work are not only useful for MTES systems, but learnings, new insights and property estimates are also useful for storage application in both aquifers (ATES) and borehole (BTES) thermal energy storage system setting. BTES is a valuable technology is cases where the reservoir permeability is limited, or the water chemistry is not favourable. In this setting, the thermal properties of the lithologies have a key control on the subsurface heat storage and recovery potential. The heat injection experiment at UKGEOS showed that DTS, combined with modelling, showed that mudstone/claystone lithologies with conductivities of 1.1 – 2.4 W/(m.K) and rates of 10–15 W/m^2 have potential for longer term thermal storage. On the contrary, sandstone lithologies with higher conductivities (c. 3.5 W/(m.K)) may be more suited to shorter duration recharge/discharge cycles. These estimates however highly depend on a good estimate of the borehole material properties and are essential when implementing seasonal injection and assessing the efficiency of heat resupply over successive cycles (Wang et al., 2025).

These findings highlight the necessity to optimise the thermal properties of the borehole materials depending on the application. For BTES applications, high casing thermal conductivity will promote heat transfers through the borehole walls and storage in the overburden rock mass, depending on their thermal properties. In open loop heat storage, insulating materials will prevent heat losses as the water is flowing in the borehole, promoting storage in and around mine workings (Gascuel et al., 2024).

5. Conclusion

Numerical modelling with COMSOL Multiphysics was used to support the interpretation of the Distributed Temperature Sensing data acquire in an injection borehole during a 17-day heat injection experiment at the UK Geoenergy Observatory in Glasgow and better constrain the subsurface properties and storage potential of mine water reservoirs. 1D approaches were first used to investigate the relative effect of the borehole design and the borehole and rock properties on the temperature signal measured during injection and heat recovery. The 2D model then allowed accounting for a more complex geometry, including the heterogeneities in the lithological succession, vertical heat transfers and groundwater flow in the GU mine working. This work is, to the best of our knowledge, the first time that a heat injection experiment and subsequent analysis of DTS data to constrain the subsurface properties has been conducted in a flooded coal mine.

The results showed that borehole casing, grout and rock thermal conductivity have an interdependent control on the heat transfer. The short-term response in the overburden rock mass highly depends on the borehole construction / material properties, whist the long-term signal is dependent on the overburden rock properties. Sandstone lithologies with a thermal conductivity of 3.4 W/(m.K) showed steady rates of heat charge of c. 23 W/m^2 (with a maximum rate of temperature change ΔT of 0.86°C/d at the start of heat injection) and discharge rates of up to 14 W/m^2 at the start of recovery (with an average recovery rate of -0.28°C/d). Clays with $\lambda_r = 1.2$ W/m^2 showed steady charging rates of c.16 W/m^2 (with a maximum ΔT of 1.02°C/d at the start of heat injection) and maximum discharge rates of c. 10 W/m^2 at the end of recovery (with an average recovery rate of -0.48°C/d).

The findings show that lithology variations in the rock mass also influence vertical conductive heat transport processes under heat storage and heat recovery. Vertical heat transfers were shown to play a key role during heat recovery, impacting the rate at which the system returns to an equilibrium. Evidence of conductive vertical heat transfer from the mine workings over longer timescales was also interpreted from the progressive upward diffusion of heat, critical to the charging/discharging of thermal battery over a wider volume. These suggest that accounting for heterogeneities throughout the lithological succession is essential to understand the overall temperature profile and refine the rocks thermal conductivity.

Discrepancies between the modelled temperature and the DTS data were observed and interpreted to result both from the model simplifications and the hydraulic processes (i.e. groundwater flow, convection in the borehole). Further work should therefore consider these factors, including the use of automatic parameter estimation, process coupling, and take the advantage of other existing datasets (e.g. electrical resistivity tomography) to better constrain the properties, controls on heat recovery and potential effect of fracturing around the mine workings. These results have applicability to Carboniferous coalfield successions common underlying many UK towns and cities.

Funding

This research was funded by the EPSRC, United Kingdom grant number EP/V042564/1 Geothermal Energy from Mines and Solar-Geothermal heat (GEMS).

CRediT authorship contribution statement

Mylene Receveur: Writing – original draft, Visualization, Software, Methodology, Investigation, Formal analysis, Data curation, Conceptualization. **Andres Gonzalez Quiros:** Writing – review & editing, Visualization, Validation, Supervision, Software, Resources, Methodology, Investigation, Formal analysis, Data curation, Conceptualization. **Alison Monaghan:** Writing – review & editing, Validation, Supervision, Project administration, Funding acquisition. **Vanessa Starcher:** Writing – review & editing, Project administration, Funding acquisition. **Kyle Walker-Verkuil:** Writing – review & editing, Resources. **David Boon:** Writing – review & editing, Resources. **Jeroen van-Hunen:** Writing – review & editing, Validation, Project administration, Funding acquisition.

Declaration of competing interest

The authors declare the following financial interests/personal relationships which may be considered as potential competing interests:

Mylene Receveur reports financial support was provided by UK Research and Innovation. If there are other authors, they declare that they have no known competing financial interests or personal relationships that could have appeared to influence the work reported in this paper.

Acknowledgment

We thank Christopher Brown as well as *Geothermics'* reviewers and editor for the insightful comments and feedback on the manuscript.

Data availability

All data were collected at the UK Geoenergy Observatory in Glasgow and may be provided upon request. Please visit the UKGEOS website to access and download open data.

References

Acuña, J., Palm, B., 2013. Distributed thermal response tests on pipe-in-pipe borehole heat exchangers. Appl. Energy 109, 312–320.
Adams, R., Younger, P., 2001. A strategy for modeling ground water rebound in abandoned deep mine systems. Groundwater 39, 249–261.
Aminossadati, S.M., Mohammed, N.M., Shemshad, J., 2010. Distributed temperature measurements using optical fibre technology in an underground mine environment. Tunnel. Undergr. Space Technol. 25, 220–229.
Andrews, B.J., Cumberpatch, Z.A., Shipton, Z.K., Lord, R., 2020. Collapse processes in abandoned pillar and stall coal mines: Implications for shallow mine geothermal energy. Geothermics 88, 101904.
Arnon, A., Selker, J., LENSKY, N., 2016. Thermohaline stratification and double diffusion diapycnal fluxes in the hypersaline Dead Sea. Limnol. Oceanogr. 61, 1214–1231.
Atkinson, T., Mcling, T., Egert, R., Jin, W., Doughty, C., Dobson, P., Oldenburg, C., Zhang, Y., Kneafsey, T. & Mcdermott, C. 2024. Galleries-to-Calories (G2C): an international collaboration evaluating thermal energy storage in abandoned mines for district heating.
Bailey, M., Moorhouse, A., Watson, I., 2013. Heat extraction from hypersaline mine water at the Dawdon mine water treatment site. Mine Closure 2013. In: Proceedings of the Eighth International Seminar on Mine Closure. Australian Centre for Geomechanics, pp. 559–570.
Beier, R.A., Acuña, J., Mogensen, P., Palm, B., 2012. Vertical temperature profiles and borehole resistance in a U-tube borehole heat exchanger. Geothermics. 44, 23–32.
Blume, T., Krause, S., Meinikmann, K., LEWANDOWSKI, J., 2013. Upscaling lacustrine groundwater discharge rates by fiber-optic distributed temperature sensing. Water. Resour. Res. 49, 7929–7944.
Brown, C.S., Kolo, I., Lyden, A., Franken, L., Kerr, N., Marshall-Cross, D., Watson, S., Falcone, G., Friedrich, D., Diamond, J., 2024. Assessing the technical potential for underground thermal energy storage in the UK. Renew. Sustain. Energy Rev. 199, 114545.
Browne, M., Mcmillan, A., 1989. Quaternary geology of the Clyde valley. British Geological Survey.
Comsol, 2023. COMSOL Multiphysics® v. 6.2. Programming Reference Manual COMSOL AB, Stockholm, Sweden.
Cottingham, C., Vitale, M., Selker, J., Selker, F., Lupton, S., 2013. Using fiber optics and vibrating wire piezometers to characterize an aquifer in preparation for ground and aquifer freezing. In: Proc. Annu. Conf. Int. Mine Water Assoc, pp. 111–116.
Dalla Santa, G., Peron, F., Galgaro, A., Cultrera, M., Bertermann, D., Mueller, J., Bernardi, A., 2017. Laboratory measurements of gravel thermal conductivity: An update methodological approach. Energy Procedia 125, 671–677.
Duarte, J., Rodrigues, F., Castelo Branco, J., 2022. Sensing technology applications in the mining industry—a systematic review. Int. J. Environ. Res. Public Health 19, 2334.
Farr, G., Busby, J., Wyatt, L., Crooks, J., Schofield, D., Holden, A., 2021. The temperature of Britain's coalfields. Q. J. Eng. Geol. Hydrogeo 54 qjegh2020-109.
Ferket, H.L., Laenen, B.J., Van Tongeren, P.C., 2011. Transforming flooded coal mines to large-scale geothermal and heat storage reservoirs: what can we expect. In: Proc. IMWA Congress, pp. 171–175.
Findlay, C., Mcdonald, B., Cunningham, J., 2020. A history of coal mining in Rutherglen and Cambuslang. Colin Findlay, Bob McDonald, Joe Cunningham.
Fraser-Harris, A., Mcdermott, C.I., Receveur, M., Mouli-Castillo, J., Todd, F., Cartwright-Taylor, A., Gunning, A., Parsons, M., 2022. The geobattery concept: a geothermal circular heat network for the sustainable development of near surface low enthalpy geothermal energy to decarbonise heating. Earth Sci. Syst. Soc. 2, 10047.
Freifeld, B.M., Finsterle, S., Onstott, T.C., Toole, P., Pratt, L.M., 2008. Ground surface temperature reconstructions: Using in situ estimates for thermal conductivity acquired with a fiber-optic distributed thermal perturbation sensor. Geophys. Res. Lett. 35.
Fujii, H., Okubo, H., Nishi, K., Itoi, R., Ohyama, K., Shibata, K., 2009. An improved thermal response test for U-tube ground heat exchanger based on optical fiber thermometers. Geothermics. 38, 399–406.
GALE, I. 2004. Ground source heat pumps: development of GeoReports for potential site characterisation.
Gascuel, V., Rivard, C., Raymond, J., 2024. Deep geothermal doublets versus deep borehole heat exchangers: a comparative study for cold sedimentary basins. Appl. Energy 361, 122826.
Gillespie, M., Crane, E. & Barron, H. 2013. Deep geothermal energy potential in Scotland.
Gluyas, J., Adams, C., Wilson, I., 2020. The theoretical potential for large-scale underground thermal energy storage (UTES) within the UK. Energy Reports 6, 229–237.
Gonzalez Quiros, A., Macallister, D.J., Macdonald, A., Palumbo-ROE, B., Bearcock, J., Ó Dochartaigh, B., Callaghan, E., Kearsey, T., Walker-Verkuil, K., Monaghan, A., 2024. De-risking green energy from mine waters by developing a robust hydrogeological conceptual model of the UK Geoenergy Observatory in Glasgow. Hydrogeol. J. 1–23.
Gonzalez Quiros, A., Receveur, M., Monaghan, A., Starcher, V., Walker-Verkuil, K. & Van Hunen, J. 2025a. Influence of mine geometry and working type on groundwater flow and heat transport for geothermal exploitation.
Gonzalez Quiros, A., Stewart, M., Olver, T., Klein, S., Mugova, E. & Abesser, C. 2025b Challenges and opportunities for high-temperature mine thermal energy storage with focus on regulatory barriers for implementation.
Guo, P., Zheng, L., Sun, X., He, M., Wang, Y., SHANG, J., 2018. Sustainability evaluation model of geothermal resources in abandoned coal mine. Appl. Therm. Eng. 144, 804–811.
Hamdhan, I.N., Clarke, B.G., 2010. Determination of thermal conductivity of coarse and fine sand soils. In: Proceedings World Geothermal Congress. Bali Indonesia.
Henninges, J., Huenges, E., Burkhardt, H., 2005. In situ thermal conductivity of gas-hydrate-bearing sediments of the Mallik 5l-38 well. J. Geophys. Res. 110.
Leaf, A.T., 2020. A distributed temperature sensing investigation of groundwater discharge to Haskell Lake. In: Lac du Flambeau Reservation, Wisconsin, July 27–August 1, 2016. US Geological Survey.
Li, B., Zhang, J., Ghoreishi-Madiseh, S.A., De Brito, M.A.R., Deng, X., Kuyuk, A.F, 2020. Energy performance of seasonal thermal energy storage in underground backfilled stopes of coal mines. J. Clean. Prod. 275, 122647.
Lowry, C.S., Walker, J.F., Hunt, R.J., ANDERSON, M.P., 2007. Identifying spatial variability of groundwater discharge in a wetland stream using a distributed temperature sensor. Water. Resour. Res. 43.
Maciver, J., Karaulanov, R 2019. Glasgow Geothermal Energy Research Site, GGA01, Project ref. 19/01/BGSG. Silixa.
Majcin, D., Bilčík, D., Hvoždara, M., 2012. Refraction of heat flow on subsurface contrast structures–the influence both on geothermal measurements and interpretation approaches. Contri. Geophy. Geod. 42 (2), 133–159.
Mcdaniel, A., Fratta, D., Tinjum, J.M., Hart, D.J., 2018. Long-term district-scale geothermal exchange borefield monitoring with fiber optic distributed temperature sensing. Geothermics. 72, 193–204.
Menéndez, J., Ordóñez, A., Álvarez, R., Loredo, J., 2019. Energy from closed mines: underground energy storage and geothermal applications. Renew. Sustain. Energy Rev. 108, 498–512.
Metoffice, 2025. Paisley Climate Data 1959 - 2025. United Kingdom.
Monaghan, A., Barron, H., Starcher, V., Shorter, K., Walker-Verkuil, K., 2020. Mine water characterisation and monitoring borehole GGA01. UK Geoenergy Observatory, Glasgow.
Monaghan, A., Damaschke, M., Starcher, V., Fellgett, M., Kingdon, A., Kearsey, T., Hannis, S., Gillespie, M., Shorter, K. & Elsome, J. 2021. UK Geoenergy Observatories Glasgow: GGC01 cored, seismic monitoring borehole–final data release.

Monaghan, A.A., Adams, C.A., Bell, R.A., Lewis, M.A., Boon, D., González Quirós, A., Starcher, V., Farr, G., Wyatt, L.M., Todd, F., 2026. Geological factors in the sustainable management of mine water heating, cooling and thermal storage resources in the UK. In: Energy Geoscience Conference Series. The Geological Society of London, London egc1-2023-39.

Monaghan, A.A., Bateson, L., Boyce, A.J., Burnside, N.M., Chambers, R., De Rezende, J. R., Dunnet, E., Everett, P.A., Gilfillan, S., Jibrin, M.S., 2022a. Time zero for net zero: a coal mine baseline for decarbonising heat. Earth Sci. Syst. Soc. 2, 10054.

Monaghan, A.A., Starcher, V., Barron, H., Shorter, K., Walker-Verkuil, K., Elsome, J., Kearsey, T., Arkley, S., Hannis, S., Callaghan, E., 2022b. Drilling into mines for heat: geological synthesis of the UK Geoenergy Observatory in Glasgow and implications for mine water heat resources. Q. J. Eng. Geol. Hydrogeo 55 qjegh2021-033.

Ngoyo Mandemvo, D.D., Comeau, F.-A., Raymond, J., Grasby, S.E., Terlaky, V., 2023. Geothermal potential of closed underground mines: resource assessment study of the Con Mine, Northwest Territories, Canada. In: Nat. Resour. Res., 32, pp. 1579–1593.

Ordóñez, A., Jardón, S., Álvarez, R., Andrés, C., Pendás, F., 2012. Hydrogeological definition and applicability of abandoned coal mines as water reservoirs. J. Environ. Monitor. 14, 2127–2136.

Passamonti, A., Bombarda, P., Pachai, A.C., Klein, S., Schneider, C., Bracke, R., 2024. Overview of a newly-installed high-temperature heat pump demonstrator coupled with high-temperature mine thermal energy storage. Int. J. Refrig. 167, 269–279.

Passamonti, A., Sachse, F., Bombarda, P., Bracke, R., 2025. Design, construction, and commissioning of a 500 kW high-temperature heat pump plant for the district heating network of Bochum, Germany. Energy Reports 13, 548–561.

Perez Silva, J., Mcdermott, C., Fraser-Harris, A., 2022. The value of a hole in coal: assessment of seasonal thermal energy storage and recovery in flooded coal mines. Earth Sci. Syst. Soc. 2, 10044.

Read, T., Bour, O., Selker, J., Bense, V., Borgne, T.L., Hochreutener, R., Lavenant, N., 2014. Active-distributed temperature sensing to continuously quantify vertical flow in boreholes. Water. Resour. Res. 50, 3706–3713.

Robertson, E.C., 1988. Thermal properties of rocks. US Geological Survey.

Sayde, C., Gregory, C., Gil-Rodriguez, M., Tufillaro, N., Tyler, S., Van de Giesen, N., English, M., Cuenca, R., Selker, J.S., 2010. Feasibility of soil moisture monitoring with heated fiber optics. Water. Resour. Res. 46.

Simon, N., Bour, O., Lavenant, N., Porel, G., Nauleau, B., Pouladi, B., Longuevergne, L., Crave, A., 2021. Numerical and experimental validation of the applicability of active-DTS experiments to estimate thermal conductivity and groundwater flux in porous media. Water. Resour. Res. 57, e2020WR028078.

Slater, L.D., Ntarlagiannis, D., Day-Lewis, F.D., Mwakanyamale, K., Versteeg, R.J., Ward, A., Strickland, C., Johnson, C.D., Lane Jr, J.W., 2010. Use of electrical imaging and distributed temperature sensing methods to characterize surface water–groundwater exchange regulating uranium transport at the Hanford 300 Area, Washington. Water. Resour. Res. 46.

Steele-Dunne, S., Rutten, M., Krzeminska, D., Hausner, M., Tyler, S., Selker, J., Bogaard, T., Van de Giesen, N., 2010. Feasibility of soil moisture estimation using passive distributed temperature sensing. Water. Resour. Res. 46.

Suárez, F., Aravena, J., Hausner, M., Childress, A., Tyler, S., 2011. Assessment of a vertical high-resolution distributed-temperature-sensing system in a shallow thermohaline environment. Hydrol. Earth. Syst. Sci. 15, 1081–1093.

Todd, F., Mcdermott, C., Harris, A.F., Bond, A., GILFILLAN, S., 2024. Modelling physical controls on mine water heat storage systems. Geoenergy 2 geoenergy2023-029.

Walls, D.B., Banks, D., Boyce, A.J., Burnside, N.M., 2021. A review of the performance of minewater heating and cooling systems. Energies (Basel) 14, 6215.

Wang, M., Guo, P., Fang, C., Bu, M., Jin, X., WANG, J., 2025. Investigation of evaluation models for geothermal resources and intermittent operation/cycle thermal storage mode in closed coal mines. Geothermics 129, 103294.

Waples, D.W., Waples, J.S., 2004. A review and evaluation of specific heat capacities of rocks, minerals, and subsurface fluids. Part 1: minerals and nonporous rocks. Nat. Resour. Res. 13, 97–122.

Watzlaf, G.R., Ackman, T.E., 2006. Underground mine water for heating and cooling using geothermal heat pump systems. Mine Water. Environ. 25, 1–14.

Younger, P.L., Banwart, S.A., Hedin, R.S., Younger, P.L., Banwart, S.A., Hedin, R.S., 2002. Mining and the water environment. Mine Water 1–63.

Zhang, F., Han, D., Qin, Y., Peng, S., Zhong, D., Tang, F., Xiang, Z., Xu, H., 2023. Optimization of the monitoring of coal spontaneous combustion degree using a distributed fiber optic temperature measurement system: field application and evaluation. Fire 6, 410.